DEC 22 1997

0830-L-02 NAS 1.29/3J : 97-12

NASA TechBriefs

National Aeronautics and
Space Administration

Electronic Components and Circuits

Electronic Systems

Physical Sciences

Materials

Computer Programs

Mechanics

Machinery

Fabrication Technology

Mathematics and Information Sciences

Life Sciences

1999-035334

INTRODUCTION

Tech Briefs are short announcements of new technology derived from the research and development activities of the National Aeronautics and Space Administration. These Briefs emphasize information considered likely to be transferable across industrial, regional, or disciplinary lines and are issued to encourage commercial application.

Availability of NASA Tech Briefs and TSP's

Distribution of NASA Tech Briefs, a monthly periodical publication, is limited to engineers in U.S. Industry and to other domestic technology transfer agents. Requests for individual Tech Briefs or for Technical Support Packages (TSP's) announced herein should be addressed to

NASA Center for AeroSpace Information
Technology Transfer Office
800 Elkridge Landing Rd.
Linthicum Heights, MD 21090-2934
Telephone No. (301) 621-0245

Please reference the three-letter, five-digit control number located at the end of each Tech Brief. Information on NASA's Technology Utilization Program, its documents, and services is also available at the same facility.

Technology Utilization Officers and Patent Counsels are located at NASA field installations to provide technology-transfer access to industrial users. Inquiries can be made by writing to NASA field installations listed below.

Technology Utilization Officers and Patent Counsels

Ames Research Center
Technology Utilization Officer
Mail Code 223-3
Moffett Field, CA 94035

Patent Counsel
Mail Code 200-11
Moffett Field, CA 94035

Goddard Space Flight Center
Technology Utilization Officer
Mail Code 702-1
Greenbelt, MD 20771

Patent Counsel
Mail Code 204
Greenbelt, MD 20771

Lyndon B. Johnson Space Center
Technology Utilization Officer
Mail Code IC-4
Houston, TX 77058

Patent Counsel
Mail Code AL3
Houston, TX 77058

John F. Kennedy Space Center
Technology Utilization Officer
Mail Stop PT-PMO-A
Kennedy Space Center, FL 32899

Patent Counsel
Mail Code PT-PAT
Kennedy Space Center, FL 32899

Langley Research Center
Technology Utilization Officer
Mail Stop 143
Hampton, VA 23665

Patent Counsel
Mail Code 279
Hampton, VA 23665

Lewis Research Center
Technology Utilization Officer
Mail Stop 7-3
21000 Brookpark Road
Cleveland, OH 44135

Patent Counsel
Mail Code LE-LAW
21000 Brookpark Road
Cleveland, OH 44135

Jet Propulsion Laboratory
Technology Utilization Officer
Mail Stop 156-211
4800 Oak Grove Drive
Pasadena, CA 91109

NASA Resident Office-JPL
Technology Utilization Officer
Mail Stop 180-801
4800 Oak Grove Drive
Pasadena, CA 91109

Patent Counsel
Mail Code 180-801
4800 Oak Grove Drive
Pasadena, CA 91109

George C. Marshall Space Flight Center
Technology Utilization Officer
Code AT01
Marshall Space Flight Center, AL 35812

Patent Counsel
Mail Code CC01
Marshall Space Flight Center, AL 35812

John C. Stennis Space Center
Technology Utilization Officer
Code HA-30
Stennis Space Center, MS 39529

NASA Headquarters
Technology Utilization Officer
Code CU
Washington, DC 20546

Assistant General Counsel for Patent Matters
Code GP
Washington, DC 20546

Dryden Flight Research Center
Technology Utilization Officer
M/S D21-31
Bldg. 4832 Whse 7
Lilly Dr.
Edwards, CA 93523

NASA TechBriefs

National Aeronautics and Space Administration

December 1997
97-12

5 Electronic Components and Circuits

11 Electronic Systems

17 Physical Sciences

25 Materials

33 Computer Programs

39 Mechanics

45 Fabrication Technology

49 Mathematics and Information Sciences

This document was prepared under the sponsorship of the National Aeronautics and Space Administration. Neither the United States Government nor any person acting on behalf of the United States Government assumes any liability resulting from the use of the information contained in this document, or warrants that such use will be free from privately owned rights.

4

BLANK PAGE

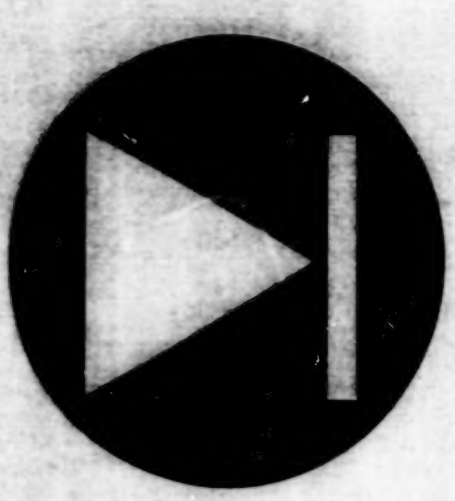

Electronic Components and Circuits

Hardware, Techniques, and Processes

7 Circular Array Antenna With Microstrip-to-Slot Transitions
8 Fixtures for Vectorial Characterization of Submillimeter-Wave Circuits
9 Power-Delay Circuit for AC-Turn-On and AC-Turn-Off Tests

BLANK PAGE

Circular Array Antenna With Microstrip-to-Slot Transitions

This relatively simple, low-profile antenna provides a toroidal radiation pattern.

Lewis Research Center, Cleveland, Ohio

Figure 1 illustrates various aspects of a low-profile microwave antenna that could be mounted on the roof of a vehicle for use in mobile/satellite communication. This antenna includes a circular array of end-fire, linearly tapered slot antenna elements. It radiates in the radial direction in the azimuth (nominally horizontal) plane, providing an overall toroidal radiation pattern with a tilt above the horizon. Unlike other low-profile antennas, this one produces the desired omnidirectional radiation pattern, without need for phase shifters or scanning mechanisms. Other advantages of this antenna include high element gain, operation over a wide frequency band, equal beam width in two orthogonal planes by proper choice of flare angle, and simple construction.

The tilt above the horizon is achieved by placing the array above a ground plane, which also simulates the metal roof of a vehicle. The antenna is connected to a coaxial cable at its center via a modified OS-50 coaxial connector that surface-launches the microwave power. A microstrip feed network of T-junctions and right-angle bends constitutes a 16-way power splitter between the coaxial cable and the 16 radial strip lines. The characteristic impedance of the microstrip lines is 50 Ω and is maintained throughout the splitter. Each of the 16 microstrip lines in the outermost part of the power splitter is electromagnetically coupled to one of the slots in the array. Electromagnetic coupling eliminates pin and solder connections and thereby increases reliability and lowers the cost. It also widens the operational frequency band, which is centered at a nominal frequency of 18 GHz.

The top part of Figure 2 shows H-plane radiation patterns measured with and without a metal ground plane under the antenna. In the presence of the ground plane, the pattern is displaced upward about 28° in elevation and the 3-dB angular width of the beam in elevation is about 22°. Tilting the array in elevation enables one to measure the E-plane radiation pattern; the bottom part of Figure 2 shows a typical peak pattern, in which the ripple is ±2 dB. Rotating the antenna in increments of 90° enables one to measure the E-plane pattern for each of four quadrants. The four radiation patterns are found to be very similar, demonstrating that the antenna has

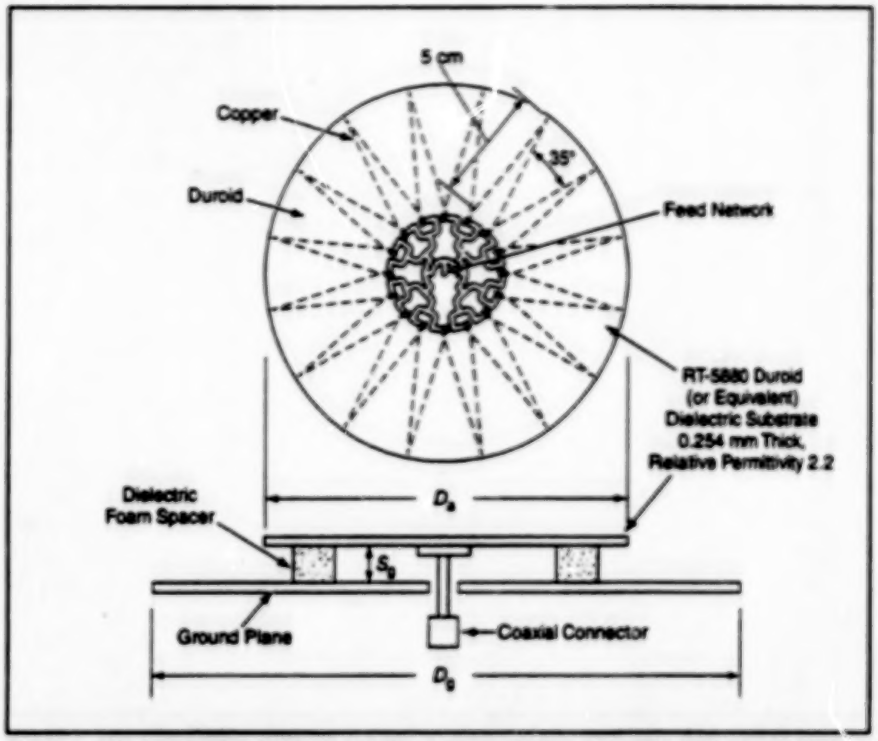

Figure 1. This Low-Profile Antenna includes a power-dividing microstrip feed network electromagnetically coupled to a circular array of 16 linearly tapered slot antenna elements. D_a = 16 cm, D_g = 30 cm, and S_g = 5 mm, which is 0.286 × the free-space wavelength at the nominal frequency of 18 GHz.

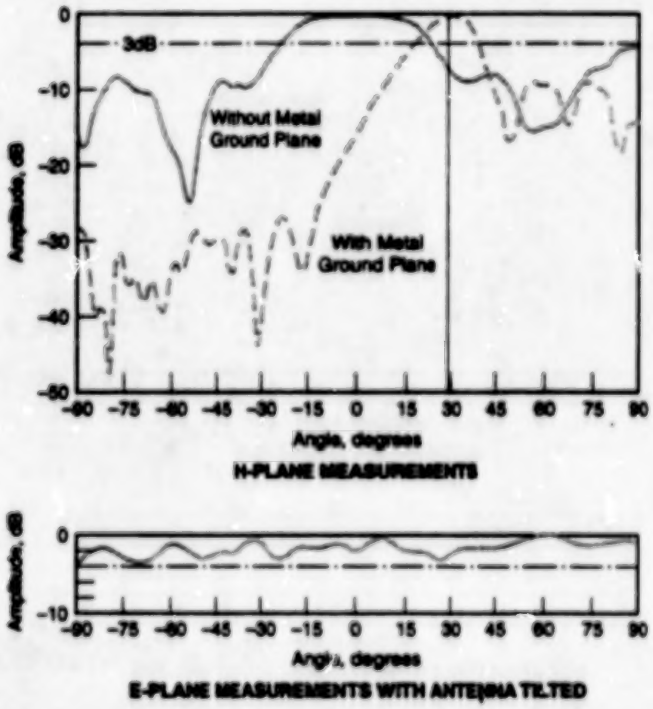

Figure 2. These Radiation Patterns indicate that the antenna has the desired directional characteristic in the elevation plane and the desired omnidirectional characteristic in the azimuth plane.

an omnidirectional characteristic in the azimuth plane.

The measured return loss of the antenna at the coaxial port is less than −10 dB (at 2:1 voltage standing-wave ratio) over the frequency range from 18 to 20 GHz. The antenna exhibits a gain of about 10 dB. The height of the antenna is less than 10 mm. By adding a four-way switch to the feed network, one could convert the antenna to multibeam operation for cellular communication.

This work was done by Richard Q. Lee and Susan Reinecke of **Lewis Research Center**, *Eron S. Kelly of Princeton University, and Rainee N. Simons of NYMA, Inc. Further information is contained in a TSP [see page 1].*

Inquiries concerning rights for the commercial use of this invention should be addressed to the Patent Counsel, Lewis Research Center [see page 1]. Refer to LEW-16283.

Fixtures for Vectorial Characterization of Submillimeter-Wave Circuits

It should soon become possible to make vectorial measurements at frequencies up to 1 THz.

NASA's Jet Propulsion Laboratory, Pasadena, California

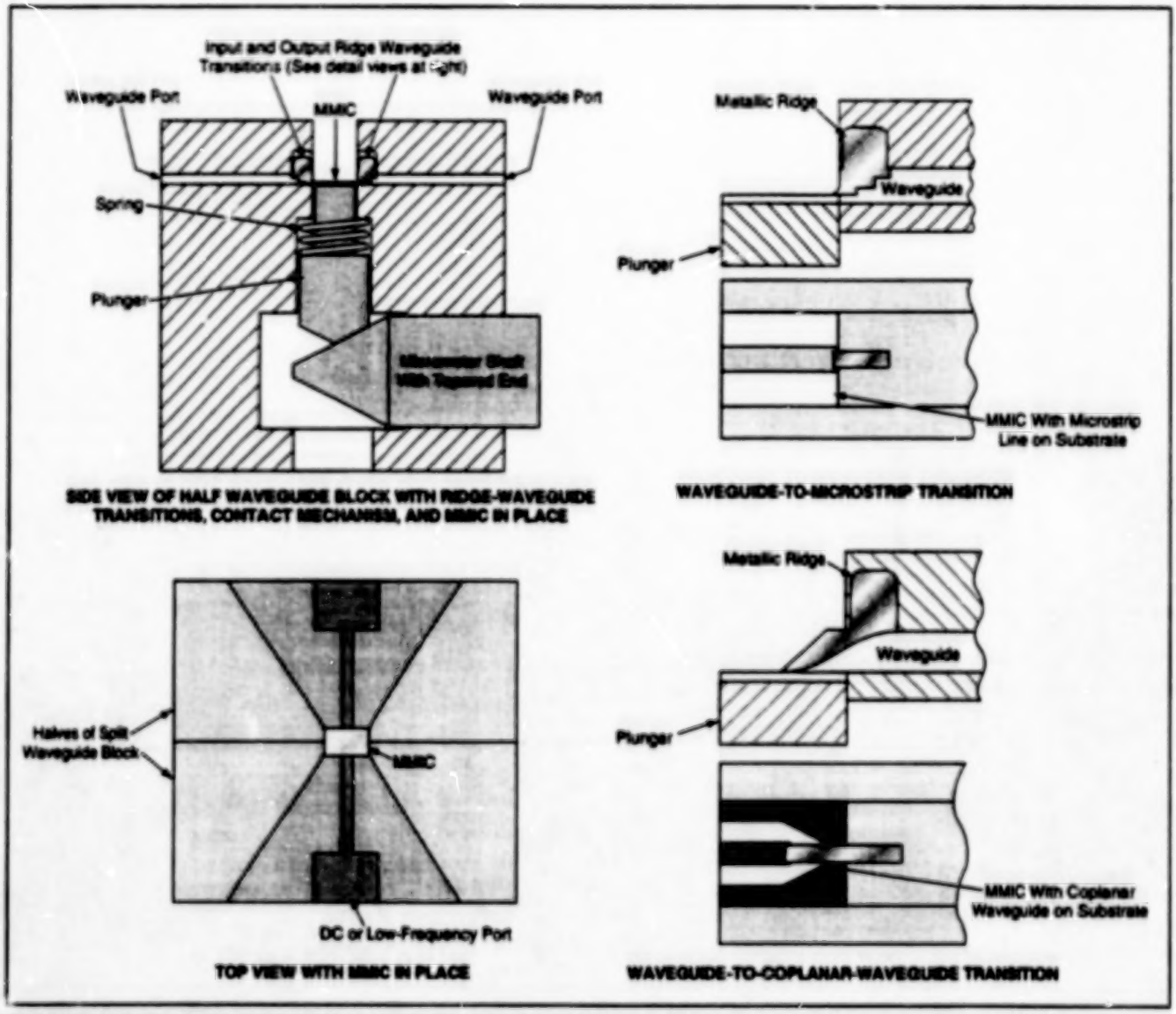

This Probe Fixture in a split waveguide block incorporates several novel features to achieve an advance in characterization of MMICs at frequencies of hundreds of gigahertz.

Convenient probe fixtures for measuring the input and output electrical characteristics of monolithic microwave integrated circuits (MMICs) at frequencies of hundreds of gigahertz are undergoing development. These fixtures contain flexible mechanisms for rapid mechanical and electrical attachment to MMICs, and provide for bias input and/or low-frequency output. Both coplanar-waveguide and microstrip versions are available. One prototype fixture is designed for frequencies up to 640 GHz, and parts of it have been tested at 160 GHz. The probe-fixture designs are frequency scalable, so that it should soon become possible to realize the potential of modern network analyzers for testing MMICs at frequencies up to 1 THz.

A probe fixture of this type (see figure) includes a housing in the form of a split waveguide block. The split waveguide configuration makes it fairly easy to machine waveguides. Fabrication and setup are simplified further by making the input and output ports collinear.

Unlike in a typical probe fixture designed for lower frequencies, radio-frequency contact with an MMIC to be characterized is not effected with a coaxial microstrip or coplanar-waveguide probe. Instead, radio-frequency contact with the MMIC device is made via two ridge waveguide transitions, which are of either (a) a waveguide-to-coplanar-waveguide design or else (b) a waveguide-to-microstrip design, depending on the nature of the MMIC device to be characterized. The ridge waveguide transitions are fabricated on thin metallic sheets by a photolithographic etching process, and are then mounted permanently in the waveguide block.

The MMIC to be characterized is placed on a spring-loaded plunger, which is used to contact nondestructively the ridge transitions with pads on the surface of the MMIC chip. A micrometer is used to pressurize the spring contact accurately. Access to the MMIC for bias or low-frequency input/output is provided by radio-frequency-isolated, microstrip-style conductors within the waveguide block in the plane of the MMIC chip. These conductors are terminated in wire bonds to the MMIC chip and in SMA connectors mounted to the outside of the waveguide block.

This work was done by Jean Bruston, Peter H. Siegel, and Pete Bruneau of Caltech for **NASA's Jet Propulsion Laboratory**. *Further information is contained in a TSP [see page 1].*

NPO-19949

Power-Delay Circuit for AC-Turn-On and AC-Turn-Off Tests

Turn-on and turn-off delays are selectable at phase resolution of 10°.

Lewis Research Center, Cleveland, Ohio

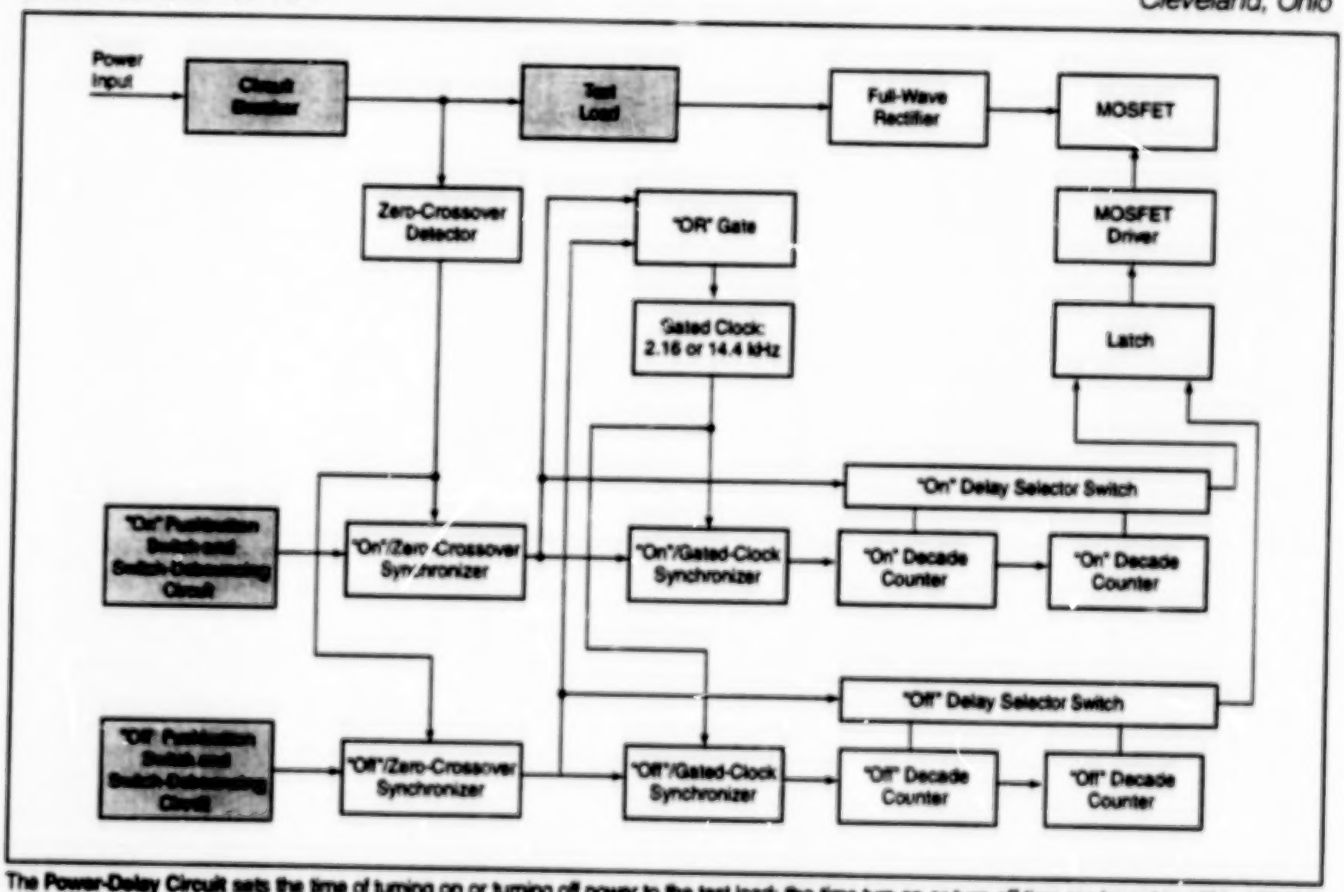

The Power-Delay Circuit sets the time of turning on or turning off power to the test load; the time turn-on or turn-off time can be set to within 1/36 of a cycle at a power-line frequency of either 60 or 400 Hz.

A power-delay circuit has been designed for use in ac-turn-on (inrush) and ac-turnoff tests of other electronic equipment. Standard testing for electromagnetic interference includes such tests. Inrush tests pertain to (a) the transient current drawn when a piece of equipment is initially turned on and (b) the effect of this transient current on the power-line voltage. In another transient associated with turnoff, power is reflected back to the source. In the case of dc equipment, the constancy of the supply voltage makes turn-on and turn-off testing a fairly straightforward problem. In the case of ac equipment, the periodicity of the supply voltage complicates the testing problem.

The power-delay circuit itself operates from 120 Vac. The input to the load under test may be any ac line voltage up to 120 V at a maximum peak load of 20 A at either 60 or 400 Hz. The rise and fall times of the switched load current are less than 5 μs. The circuit enables the tester to choose any turn-on delay in the phase range of 0 to 360°, with a resolu-

tion of 10°, at either power-line frequency.

The circuit (see figure) was designed around readily available components for convenience. A zero-crossover detector generates a pulse each time the instantaneous power-line potential crosses from a negative to a positive value. The zero-crossover pulse is optically coupled to a pair of synchronizers, along with the outputs of either an "on" or an "off" push-button-switch/debouncing-circuit unit. The outputs of the affected synchronizer is a pulse synchronized with a zero crossover.

A clock gated by the "on" or "off" zero-crossover synchronizer pulse generates a square wave at a frequency of 2.16 kHz for a 60-Hz power line, or else 1.4 kHz for a 400-Hz power line. This gated clock is what provides the 10° phase resolution. One in another pair of synchronizers generates an "on" or "off" signal synchronized to the gated clock signal. The "on" or "off" signal is counted to the selected delay by a pair of cascaded decade counters synchronized to the gated clock.

The "on" or "off" signal is routed to a latch that holds off the power to the test load until the desired turn-on time, then keeps the power to the load turned on until the latch is reset by the "off" delay circuit. The output of the latch drives "on" and "off" indicator light-emitting diodes and is optically coupled to a driver for a metal oxide semiconductor field-effect transistor (MOSFET). Inasmuch as a MOSFET is a dc device, a bridge rectifier comprising ultra-fast-recovery diodes is used to enable switching of the input ac power with the MOSFET. An ultra-fast-recovery diode is used as a flyback device to improve the fall time of the circuit.

This work was done by Dennis Eichenberg and Noel B. Sargent of **Lewis Research Center** *and Michael Herlacher of Cortez III. No further documentation is available.*

Inquiries concerning rights for the commercial use of this invention should be addressed to NASA Lewis Research Center, Commercial Technology Office, Attn: Tech Brief Patent Status, Mail Stop 7-3, 21000 Brookpark Road, Cleveland, Ohio 44135. Refer to LEW-16452.

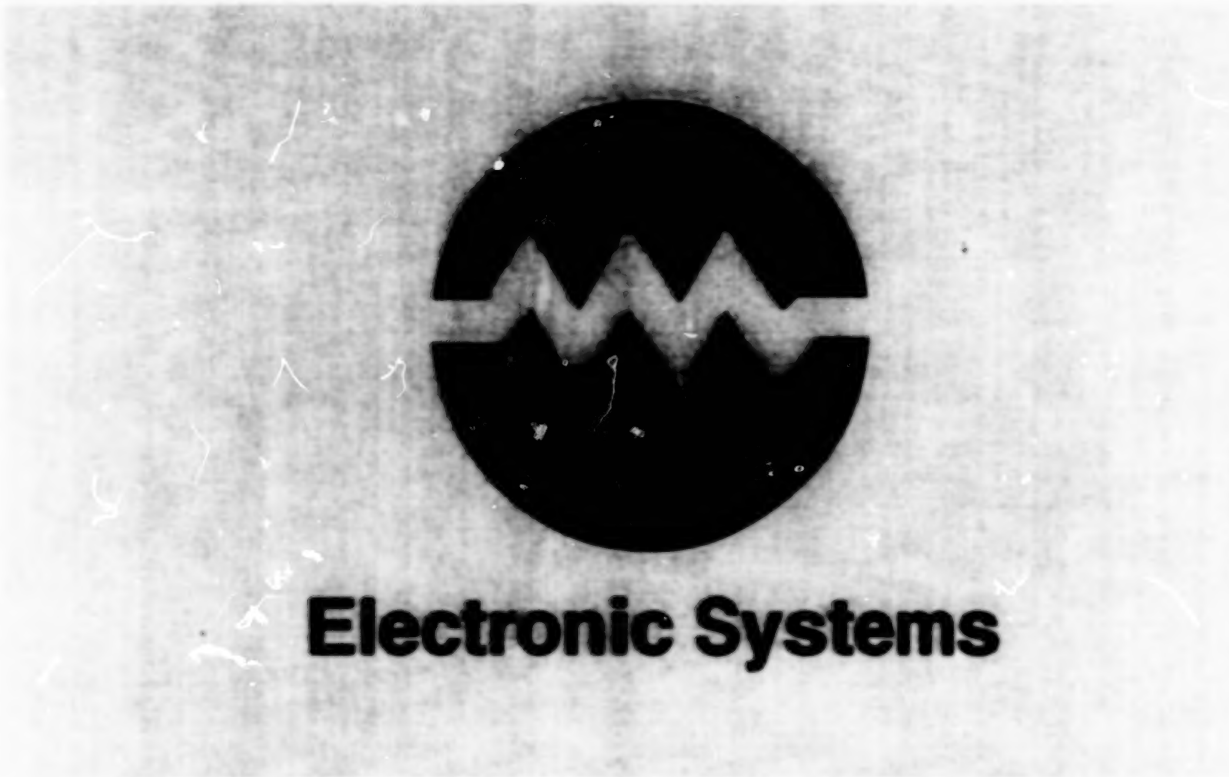

Hardware, Techniques, and Processes

13 High-Resolution Decoder for Multianode Detectors
14 Neuroprocessor for Detecting Misfire in an Automotive Engine

BLANK PAGE

High-Resolution Decoder for Multianode Detectors

Resolution is doubled by discriminating between even- and odd-fold anode pulses.

Goddard Space Flight Center, Greenbelt, Maryland

An improved decoding circuit for a multianode microchannel-array (MAMA) detector doubles the spatial resolution over that previously available, without loss of temporal resolution. As explained below, it does this by a scheme that includes parallel processing of a least-significant bit, indicative of the pixel location, during the normal signal-processing period.

The MAMA is a photon-counting detector that employs a photocathode for photon/electron conversion and a microchannel plate for electron multiplication. The output of the microchannel plate is taken in the form of pulses of electrons that impinge on an array of crossed sets of interdigitating anodes (see Figure 1). The anodes shown determine the horizontal position of a photon event. The vertical position is determined by another pair of interdigitating anode sets (not shown), which run underneath and perpendicular to the first pair of anode sets. Charge amplifier circuits amplify the signals detected by the anodes. A digital decoder circuit interprets the outputs to determine the position of an event. The decoder does this through coincidence discrimination, which is the process of identifying two or more contiguous anodes that experience electron pulses that are coincident in time and inferring the pixel location of an event.

As shown at the bottom of Figure 1, a photon can give rise to simultaneous pulses in two or more adjacent anodes in one of the crossed sets; such a pulse is known in the industry as an "*n*-fold," where *n* denotes the number of anodes involved. Also, note that a pixel is bounded along one axis by the centerlines of two adjacent anodes. For purposes of determining position, any *n*-fold with *n* even and $n > 2$ can be reduced by the decoding circuitry to an equivalent 2-fold that occupies the same central pixel as does the *n*-fold. However, an *n*-fold with *n* odd could be converted to an equivalent 2-fold that could be assigned to either one of two adjacent pixels. This affords an opportunity to halve the effective pixel size (double the resolution by assigning the equivalent 2-fold to the position midway between the pixels).

The improved decoder is fabricated as an application-specific integrated circuit (ASIC). This ASIC discriminates between even-folds and odd-folds to generate a single least-significant bit indicative of half the pixel interval that was available previously.

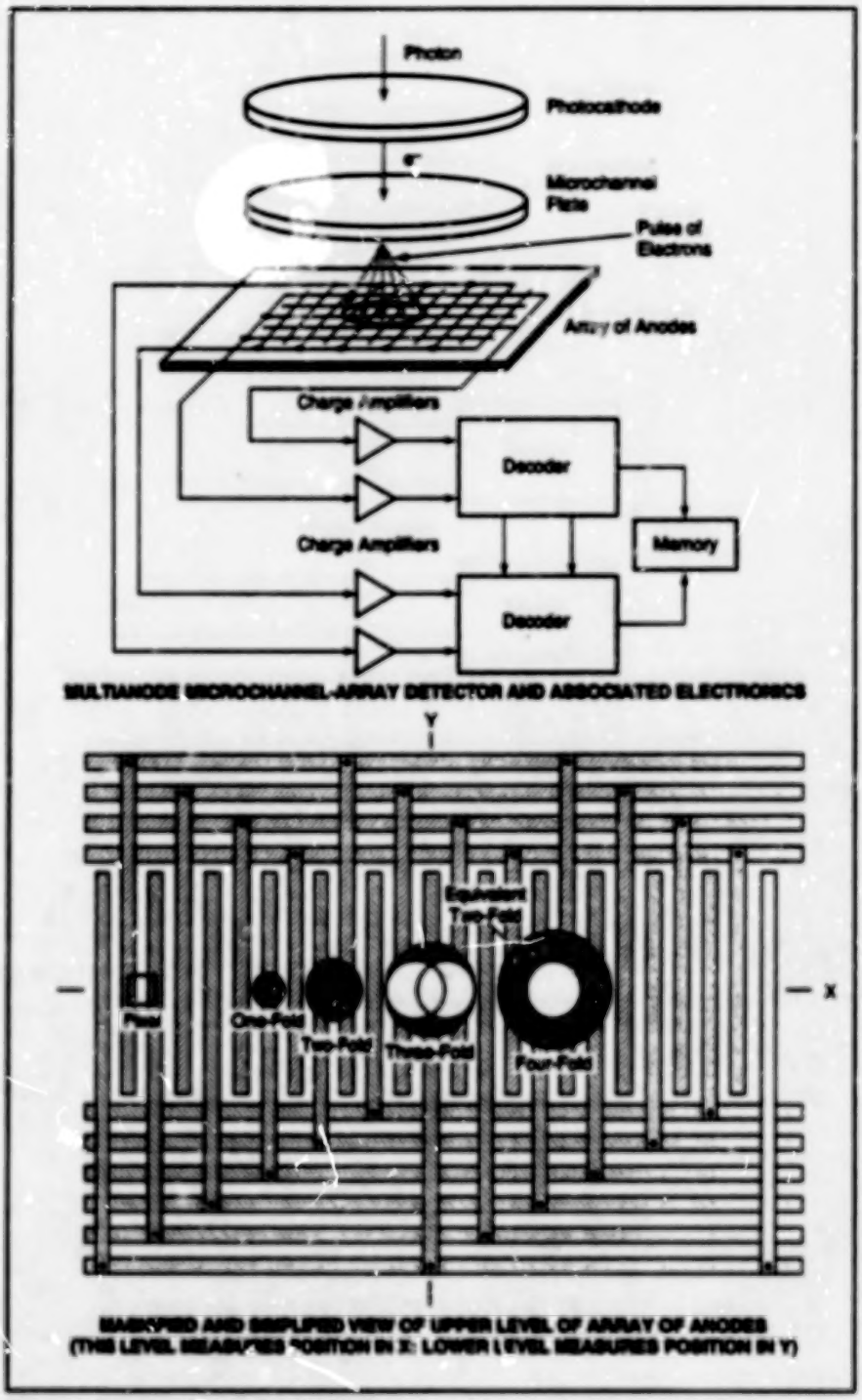

Figure 1. Decoders Determine the Position of a photon by coincidence discrimination among pulses of electrons collected by an array of anodes.

This operation is performed in parallel with the standard decoding, with no loss of decoder speed, and necessitates the addition of minimal hardware to the standard decoding circuitry. (However, the size of the memory must be quadrupled.)

High-resolution decoding dramatically improves image quality, as illustrated in Figure 2, which shows a normal low-resolution image of a portion of a USAF test target and a high-resolution image of the

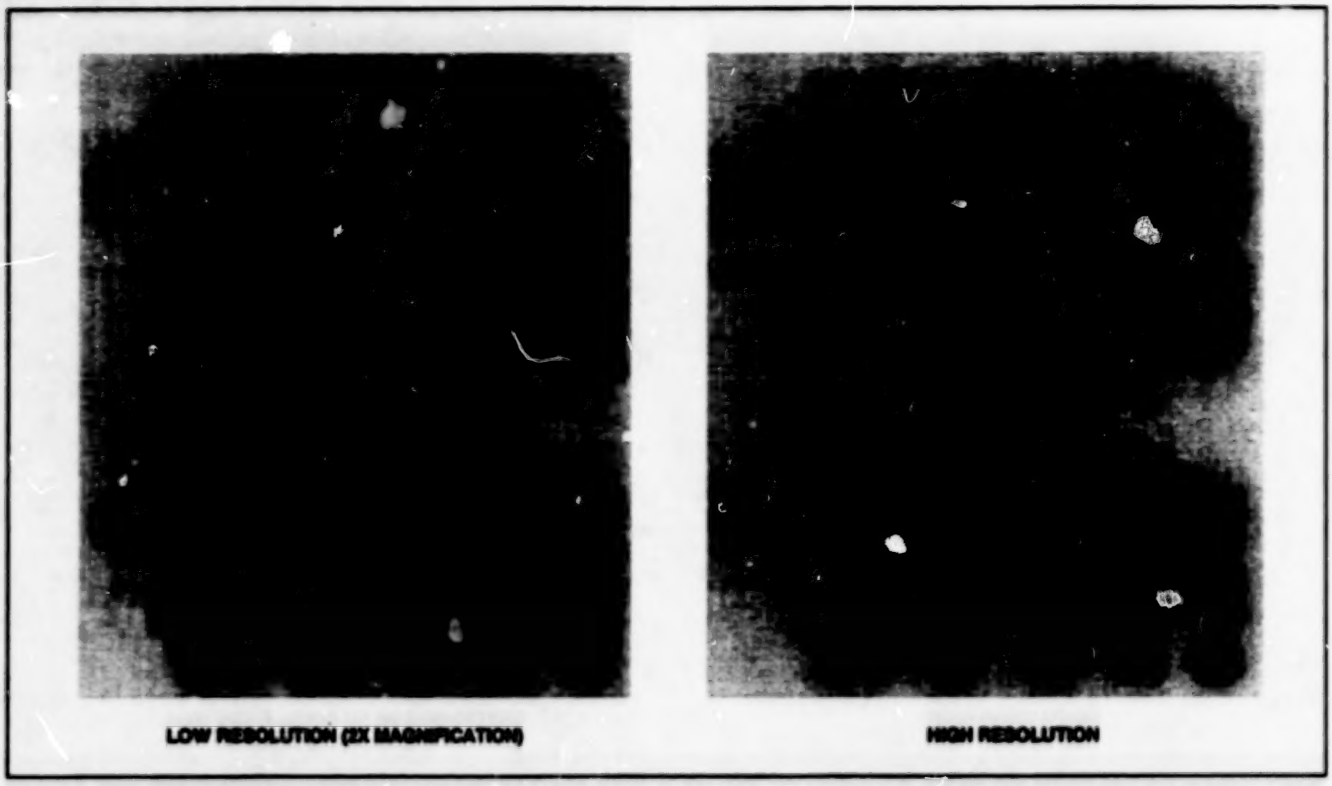

Figure 2. High-Resolution Decoding produces superior image shown on the right. For comparison, the left side shows normal-resolution image (2× magnification) of a portion of a USAF test target.

same target. The high-resolution image resolves much smaller features and displays greater detail. The images were recorded with a 16-bit depth, but they are displayed in an 8-bit mode. Therefore, the brightest areas of the images, such as the inner portions of the largest rectangles, experience "roll-over" in the displayed image.

This work was done by David B. Kasle of **Goddard Space Flight Center.** *Further information is contained in a TSP [see page 1].*

This invention is owned by NASA, and a patent application has been filed. Inquiries concerning nonexclusive or exclusive license for its commercial development should be addressed to the Patent Counsel, Goddard Space Flight Center [see page 1]. Refer to GSC-13478.

Neuroprocessor for Detecting Misfire in an Automotive Engine

Indications of misfire are derived from crankshaft-acceleration and other sensory inputs.

NASA's Jet Propulsion Laboratory, Pasadena, California

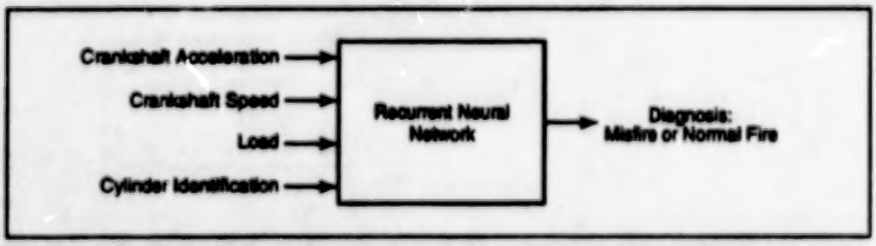

Figure 1. A Neural Network with time-lagged feedback in two hidden layers processes four sensory inputs to obtain indications of misfire.

An application-specific integrated circuit (ASIC) has been developed as a prototype of neuroprocessors for detecting misfire in internal-combustion piston engines. Such neuroprocessors are intended to satisfy a requirement, imposed by the Federal government pursuant to the Clean Air Act, to equip automobiles with onboard diagnostic capabilities that include a misfire-detection capability.

Engine misfire is defined as incompleteness or absence of combustion in a given cylinder at its intended time of firing. Misfire causes a diminution or loss of the torque pulse that the firing is intended to produce, giving rise to a deficit in crankshaft torque or acceleration. The detection of an acceleration deficit is the basis for detecting a misfire, but the detection problem is complicated in that the acceleration-deficit signal is obscured by crankshaft torsional oscillations, which are dominated by the more-frequently-occurring normal combustion events. A neuroprocessor was chosen for this diagnostic task because engine-control microprocessors now in common use cannot efficiently perform the complex mathematical operations necessary to extract misfire signals from the outputs of engine sensors.

The neuroprocessor receives four sensory inputs (see Figure 1), of which two are crankshaft speed and acceleration signals, computed as time derivatives of the output of a crankshaft-angular-position sensor; these derivatives are computed at small crankshaft-angle intervals between nominal firings. The third sensory input is an

indication of which cylinder firing is the one currently under observation; this input may not be strictly necessary, but is desirable in that it provides relatively clean phase information and enables the neuroprocessor to synchronize itself more rapidly with engine cycles as operating conditions change. The fourth sensory input is an engine-load signal.

The neuroprocessor is characterized as a recurrent neural network with four inputs (not counting a bias input), 20 time-lagged recurrent nodes (neurons) in a first hidden layer, 10 time-lagged recurrent nodes in a second hidden layer, and a single output node. The neuroprocessor ASIC is implemented in high-speed complementary metal oxide/semiconductor (CMOS) very-large-scale integrated (VLSI) circuitry with a bit-serial architecture, which makes for compactness and cost-effectiveness because (1) it entails fewer interconnections and less hardware than does bit-parallel architecture and (2) it involves the periodic, repetitive use of the same circuitry in a time multiplexing scheme to implement successive layers in the neural network (see Figure 2). Such an architecture is feasible in the automotive diagnostic application because the engine speeds are low enough and the electronic circuitry operates rapidly enough that all electronic neural-network processes for a given input/output sampling period can be completed before the beginning of the next period.

The neural network is trained by the dynamic back-propagation method, using data from known normal-fire and misfire events under a large variety of operating conditions. The target output for the neuroprocessor is a +1 or a −1, according to whether or not the processing of inputs reveals a misfire 8 time steps earlier. The 8-time-step offset was found, in preliminary training trials, to enable the neural network to utilize sensory information from short-lived disturbances that persist for an engine cycle after a normal-fire or misfire events that the network is required to classify.

The foregoing combination of features affords flexibility to realize different neural-network configurations for different diagnostic functions. A neural network of this type is believed to be capable of functioning as a universal dynamic approximator in that it can be made to approximate any dynamic transfer function to arbitrary accuracy, provided that it is configured with a suitable number of nodes in hidden layers. Inasmuch as any neural network could, in principle, be composed of neural-network building-block integrated-circuit chips, this approach offers the opportunity to trade off computation speed versus cost (more chips with less time multiplexing versus fewer chips with more time multiplexing). This approach also enables the use of the same chips for multiple tasks. In effect, the number of chips needed is determined by the time constraints on the computation, and multiple tasks can be performed by storing and loading the weights for the transfer function of each task at the time of that task.

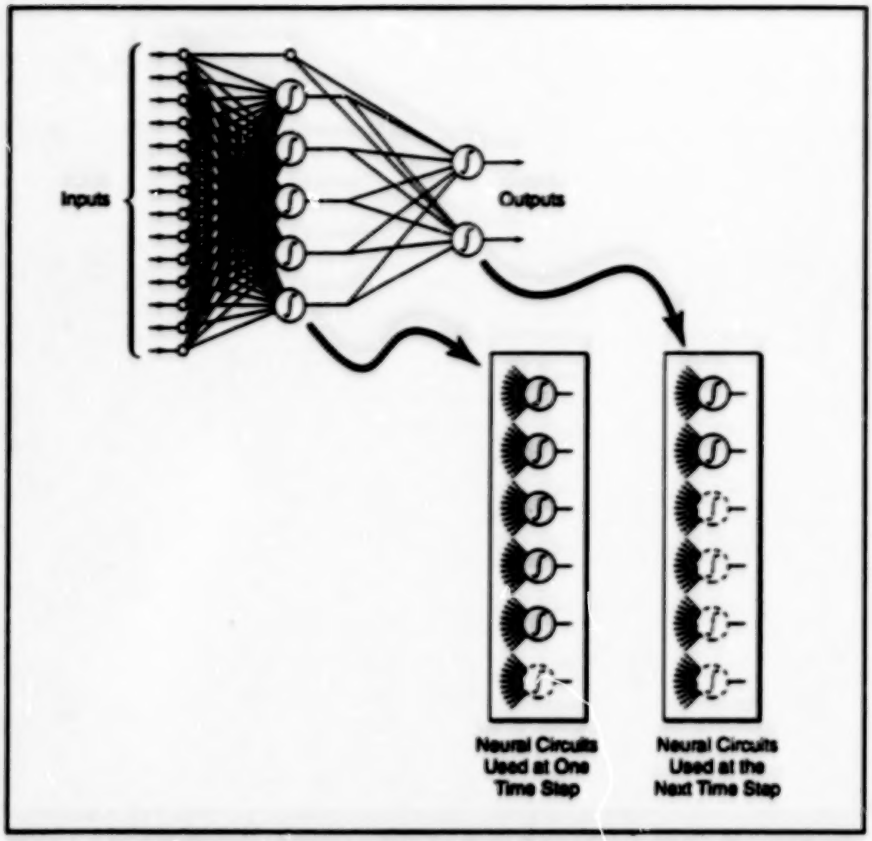

Figure 2. A Time Multiplexing Scheme enables the reuse of the same neural circuits to implement successive layers of the neural network. The neural network shown here is not the one described in the text, but, rather, a simplified feedforward neural network for the purpose of illustrating the time-multiplexing scheme.

This work was done by Raoul Tawel and Nazeeh Aranki of Caltech and Lee A. Feldcamp, Kenneth Marko, Gintaras Puskorius, and John James of Ford Motor Co. for **NASA's Jet Propulsion Laboratory.** *Further information is contained in a TSP [see page 1].*

In accordance with Public Law 96-517, the contractor has elected to retain title to this invention. Inquiries concerning rights for its commercial use should be addressed to

Technology Reporting Office
JPL
Mail Stop 122-116
4800 Oak Grove Drive
Pasadena, CA 91109
(818) 354-2240

Refer to NPO-20044, volume and number of this NASA Tech Briefs *issue, and the page number.*

BLANK PAGE

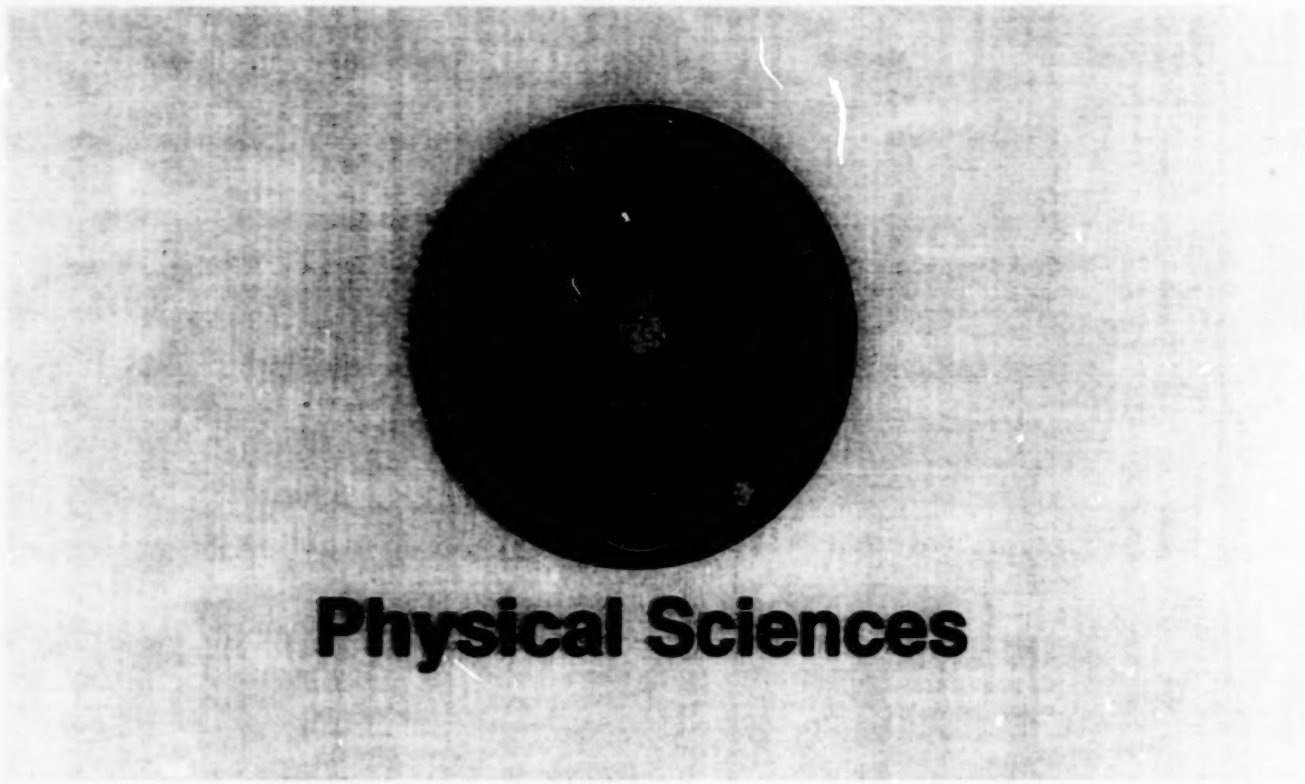

Physical Sciences

Hardware, Techniques, and Processes

19 Diode-Laser Devices for Aiming and Ranging an X-Ray Source
20 Rotational Apparatus for Heat-Transfer Experiments
21 One-Grid-Pair Fourier Telescope for Imaging X and Gamma Rays
22 Steady Capillary-Driven Flow
22 Capillary-Pumped Loops for Equalizing Body Temperatures
23 Image-Warping Coherent Fiber-Optic Bundles

Books and Reports

24 DLS Sizing of Particles in Hanging Liquid Drops
24 X-Ray-Based Strain Measurements at High Temperatures

BLANK PAGE

Diode-Laser Devices for Aiming and Ranging an X-Ray Source

Other sources of invisible radiation (microwaves, infrared, ultrasound) could also be aimed.

Marshall Space Flight Center, Alabama

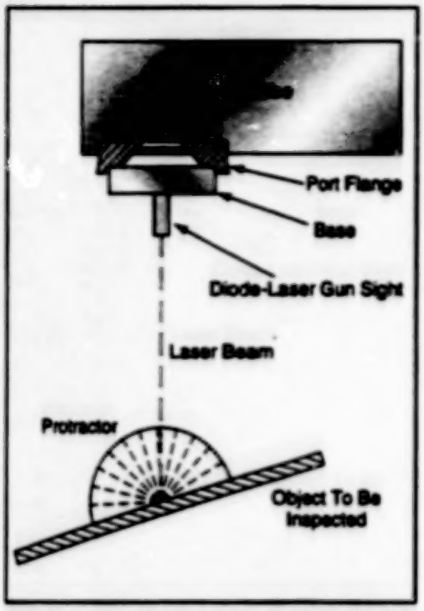

Figure 1. The Diode-Laser Aiming Device is attached temporarily to an x-ray tube and used to visibly mark the path that will later be followed by x-rays.

Two diode-laser devices have been developed to facilitate the correct positioning and orienting of an x-ray source with respect to an object to be inspected. The first of these devices is used to aim the x-ray beam toward a designated point on the object. This device is also used to measure, to within a fraction of a degree, the angle between the x-ray beam and the object surface on which the designated point lies. It is necessary to measure this angle because angular errors as small as 1° have been known to lead to incorrect interpretation of x-radiographs. The second diode-laser device is used in conjunction with the first device to measure the distance between the x-ray source and the designated point on the object. Knowledge of this distance is necessary for extracting three-dimensional position information from x-radiographs.

Laser devices have been used previously for aiming x-ray sources. The advantage of the present laser devices is relative simplicity; they contain fewer parts and are easier to use. The present aiming device (see Figure 1) comprises a diode-laser gunsight mounted on a plastic or aluminum base that has been machined to mate with the port flange of an x-ray tube. An essential part of the fabrication of this device is a prealignment procedure in which a special optomechanical alignment jig that holds a piece of x-ray film is used to position and orient the diode-laser gunsight to make the laser beam coincide with the x-ray beam. The aiming device is held on the x-ray tube by an elastic strap and can thus be installed and removed quickly and easily.

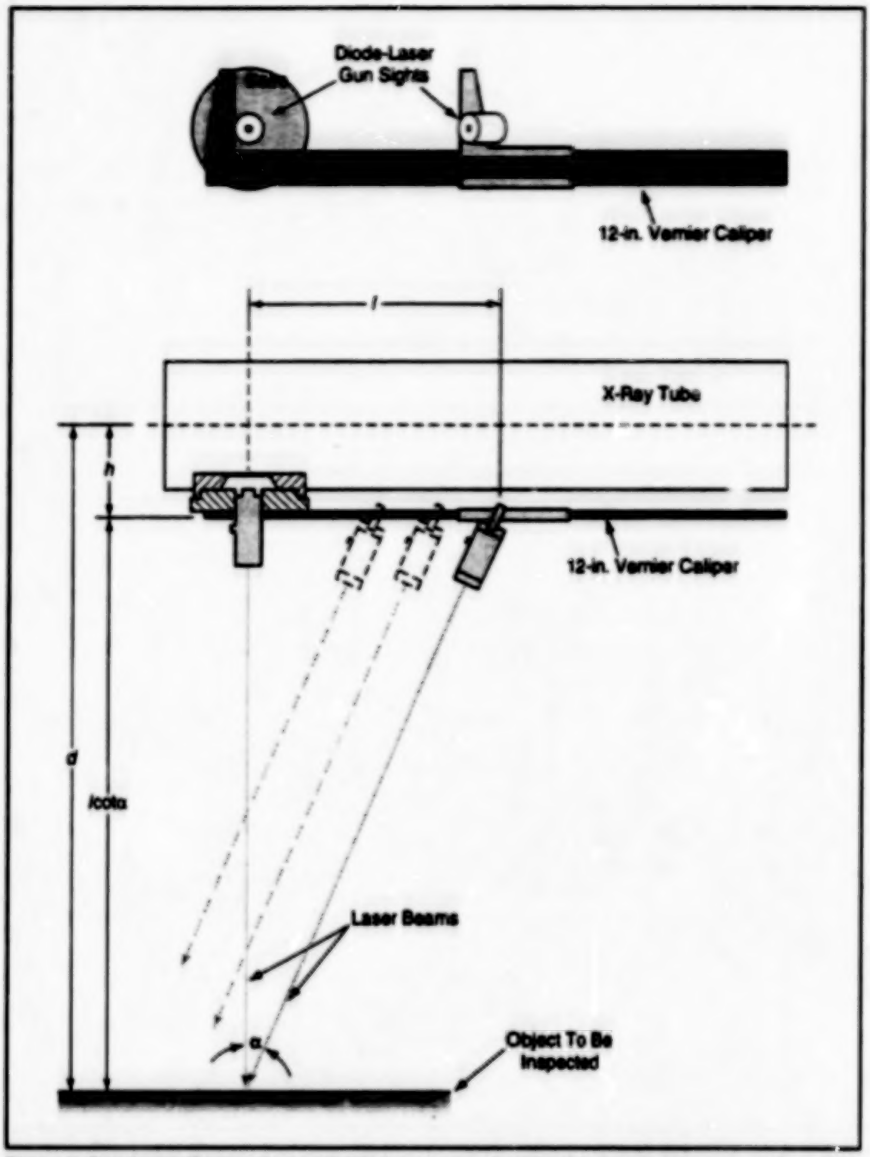

Figure 2. Two Laser Beams that originate from known locations intersect at known angle α. The distance from the axis of the x-ray tube to the object to be inspected is given by $d = h + l \cot \alpha$.

During aiming, the x-ray tube is turned off. The beam of visible light emitted by the diode laser marks the path of the x-ray beam. The position and orientation of the x-ray tube and/or the object to be inspected are adjusted until the laser-illuminated spot is centered at the designated point on the object. The angle between the beam and the surface of the object is measured by use of a protractor positioned to be grazed by the edge of the beam.

The second (distance-measuring) diode-laser device comprises another diode-laser gunsight mounted on a vernier-caliper positioning mechanism. The positioning mechanism is attached to the aiming device and used to position the second laser-beam source at a known lateral distance from the first laser-beam source. In another prealignment procedure, the second laser beam is aimed to intersect the first laser beam at a known fixed angle, regardless of the lateral-distance setting. In use, the lateral

distance is adjusted until the two beams intersect at the designated point on the object to be inspected. Then the distance between the x-ray tube and the object to be inspected can be calculated from the known lateral distance and the known angle of intersection by simple trigonometry. This device could be assembled to allow 1-in. (2.54-cm) of caliper movement to equal a 10-in. (25.4-cm) change in x-ray path length.

Modified versions of these diode-laser devices could be used to aim sources of other types of invisible radiation (microwaves, infrared, and ultrasound). Of course, the prealignment procedure for the aiming device would be different for different types of radiation.

This work was done by Glenn Cotty, Craig Clauss, and David Olson of Lockheed Martin for **Marshall Space Flight Center.** *Further information is contained in a TSP [see page 1].*
MFS-31170

Rotational Apparatus for Heat-Transfer Experiments

Data acquired in experiments could lead to improved cooling of turbine blades.

Lewis Research Center, Cleveland, Ohio

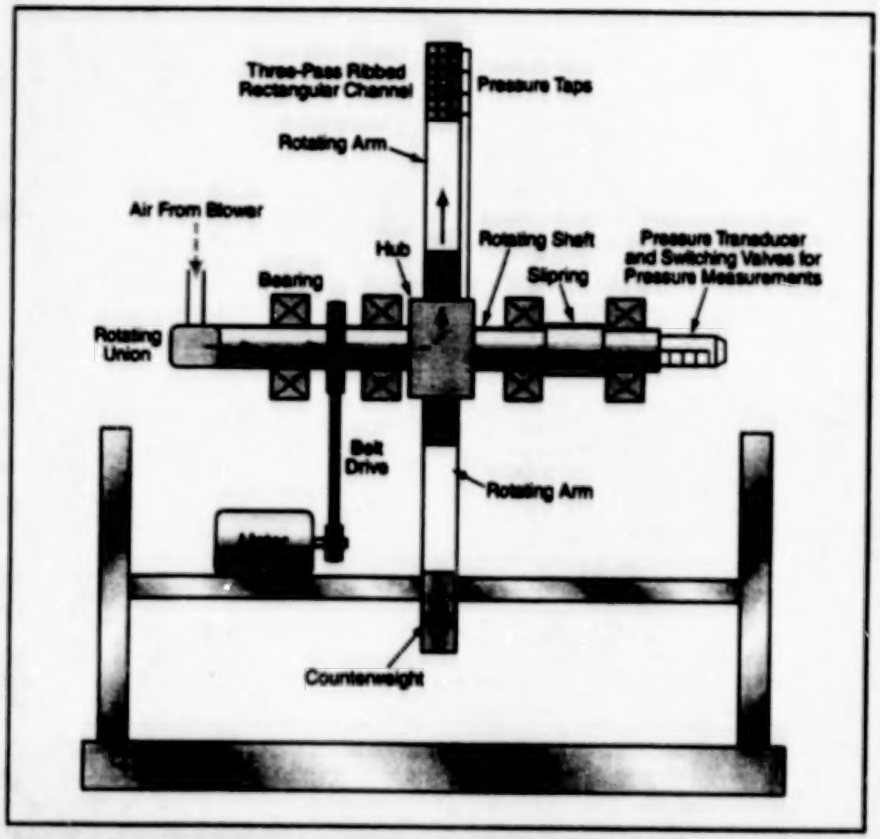

Experiments on Heat Transfer in a channel on a rotating arm would be performed to gain understanding of thermal and flow phenomena in coolant passages of gas-turbine blades.

The figure illustrates a laboratory apparatus that has been proposed for experiments on local heat transfer in and around passages in a rotating arm. The passage geometries and the flows along the passages would be chosen to model heat-transfer and flow conditions like those in the coolant passages of the blades of gas-turbine engines. It is necessary to perform such experimental modeling because there is very little published experimental information on local heat transfer (as distinguished from spatially averaged heat transfer) in passages in the presence of rotation. The data acquired in experiments on the proposed apparatus would contribute to understanding of local heat transfer in gas-turbine blades, thereby helping engineers to design blades for efficient cooling.

In a gas-turbine engine, cooling air is bled from a compressor (which is part of the engine) and directed to flow along the internal passages of the turbine blades; of course, this cooling bleed flow is obtained at the expense of total engine output. To maximize turbulence in order to maximize the transfer of heat from the blade to the cooling air, ribs are cast onto two opposite walls of each passage. Rib-induced separation and attachment of flow along the passages create zones of high and low heat transfer. Rotation aggravates the nonuniformity of heat transfer by pushing the flow onto the pressure side (where heat transfer is thus increased) and away from the suction side (where heat transfer is thus reduced). Therefore, it is necessary to determine coefficients of local heat transfer in order to identify hot spots and quantify enhancements of heat transfer on leading and trailing passage walls in the presence of rotation. Moreover, coefficients of local convective transfer of heat between hot gases and blades are greater than the thermal conductivities of the blades; thus, a blade designer cannot rely on the thermal conductivity of the blade to smooth out local errors in computed heat fluxes, and this makes it imperative to know the coefficients of local heat transfer within the blade passages in great detail.

The arm of the proposed apparatus would be designed to accommodate passages of various geometries. By use of a naphthalene-sublimation technique, local coefficients of heat and mass transfer would be determined for a variety of flow/geometry combinations, including flows in rib-roughened, multipass channels, multiple jets impinging near the leading edge of a blade, and flows around pin-fins near the trailing edge of a blade. Distributions of pressure would be measured by use of a switching-valve unit that would sequentially connect the transducer to pressure taps at various locations in the passages. A slipring assembly would be included to provide an option for conducting heat-transfer experiments.

Experiments have been conducted in a two-pass, square-cross-section channel on a small-scale prototype of the proposed apparatus, using the naphthalene-sublimation technique. Local distributions of heat and mass transfer were obtained in cases in which ribs were aligned at various angles. The most significant finding from these experiments was that high rates of heat and mass transfer on the trailing wall can be achieved with ribs smaller than those

used conventionally (hydraulic-diameter-to-rib-height ratios of 16 or 32 instead of the conventional values of 8 to 10).

This work was done by Rajesh Kukreja of Lynntech, Inc., for Lewis Research Center. Further information is contained in a TSP [see page 1].

Inquiries concerning rights for the commercial use of this invention should be addressed to NASA Lewis Research Center, Commercial Technology Office, Attn: Tech Brief Patent Status, Mail Stop 7-3, 21000 Brookpark Road, Cleveland, Ohio 44135. Refer to LEW-16337.

One-Grid-Pair Fourier Telescope for Imaging X and Gamma Rays

This telescope design provides better imaging at a significantly lower cost.

Marshall Space Flight Center, Alabama

A telescope design, using only one real and imaginary set of grid pairs, provides superior performance at a greatly reduced cost. Previous Fourier telescope designs required many fine grid pairs constructed from material such as tungsten. These multiple-grid telescopes were extremely large in order to provide a reasonable collecting area and required unreasonably long focal lengths.

The Fourier-transform design eliminates all but one set of grid pairs by incorporating rotation of the grid pairs and movement of the mass separating the two grids. This telescope has a set of subcollimators that feed discrete detectors. A measurement of the amplitude and the phase at selected points in the visual plane provides the real and imaginary parts of the Fourier component measured by a given subcollimator. A spatial modulation collimator (SMC) uses slight differences in the geometry of the grids of an aligned pair to modulate the incoming hard x-ray wave front, enabling the Fourier component to be measured. A rotating modulation collimator (RMC) uses the rotation of the instrument itself about its line of sight to provide modulation. The RMC integration time for a single frame is now linked to the rotation time of the satellite upon which the telescope is mounted. Therefore, integration time for the RMC can be significantly longer than the detection time that constrains the SMC.

Since the visibility function in the observational plane is directly related to the brightness distribution in the object plane via a Fourier transform, an image is obtained from the inverse Fourier transformation of the visibility function. A complete, well-defined image requires the measurement of the visibility function at a sufficiently dense set of points in the plane. Simulation is the best way to determine whether enough points are to be measured for a given source to provide an acceptable image.

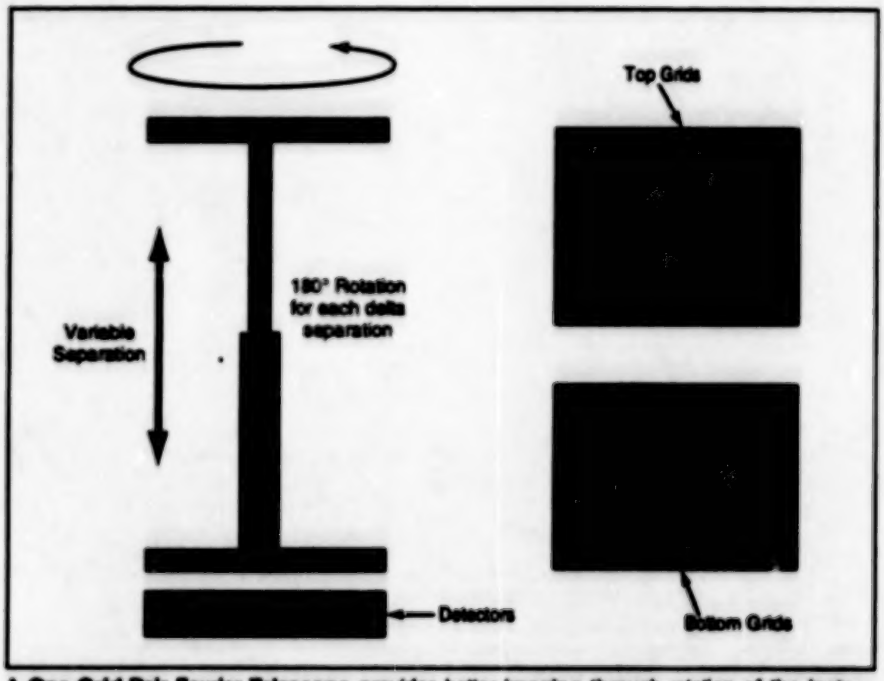

A One-Grid-Pair Fourier Telescope provides better imaging through rotation of the instrument and separation of the grid pair during operation.

Essentially, the Fourier concept involves sampling selected Fourier components from a wave front emitted by the source. Each component may be visualized by a single point on a common complex surface. By measuring a number of components over a significantly large spatial frequency spectrum, the Fourier surface may be approximated. An inverse Fourier transform of the surface function yields an approximate or "dirty" image. When viewing a typical dirty image, the processing artifacts can make the picture very difficult for the eye to see.

The Astronomical Image Processing System (AIPS), a software operating system widely used by radio astronomers, was incorporated into the simulations for the Fourier-transform telescope to clean the dirty images. This software package, which uses optional algorithms, also displayed the simulation images in a number of different ways.

Substantial progress has been made in studying x-ray and gamma-ray imaging instruments and associated support spacecraft platforms, such as the space station, the space shuttle, and Earth-orbit satellites. Through design simulations, a less-costly telescope, requiring only one set of real and imaginary grid pairs to provide better images of hard x-ray and gamma ray sources, has been developed.

This work was done by Jonathan Wesley Campbell of **Marshall Space Flight Center.** *Further information is contained in a TSP [see page 1].*

Inquiries concerning rights for the commercial use of this invention should be addressed to the Patent Counsel, Marshall Space Flight Center [see page 1]. Refer to MFS-31176.

Steady Capillary-Driven Flow

This phenomenon can be exploited to study basic physical mechanisms of dynamic wetting.

Lewis Research Center, Cleveland, Ohio

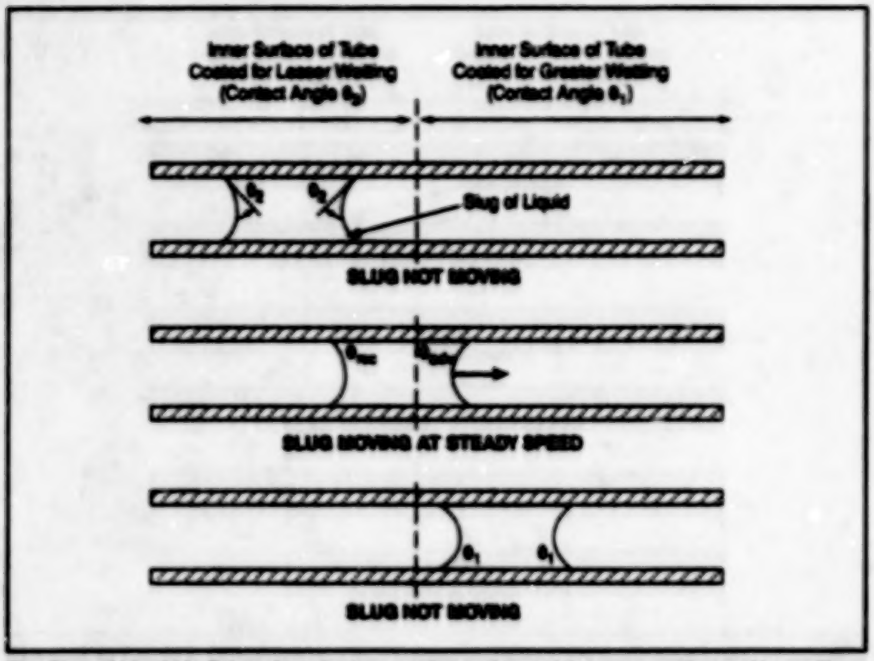
Inner Surface of Tube Coated for Lesser Wetting (Contact Angle θ_2)
Inner Surface of Tube Coated for Greater Wetting (Contact Angle θ_1)
Slug of Liquid
SLUG NOT MOVING
SLUG MOVING AT STEADY SPEED
SLUG NOT MOVING

The Slug of Liquid Is Driven from the less-wetting end toward the more-wetting end by capillary action as long as the slug straddles the θ_1/θ_2 discontinuity.

A technique for generating steady capillary-driven flow has been devised to add to the available means for studying physical mechanisms of wetting and capillary flows. Related capillary-flow techniques have been used for decades, but they have involved, variously, unsteady flows or the use of pumps, gravity heads, or other noncapillary means to generate flows. The present technique differs from the older techniques in that the flow is generated solely by capillary means; it is a truly steady flow governed by the physics of dynamic wetting.

This technique involves the movement of a slug of liquid along a round capillary tube, the inner surface of which is treated to obtain a certain degree of wetting along part of its length and greater or lesser wetting along the remainder of its length (see figure). The slug is injected into the tube at the less-wetting end, becomes accelerated in a brief transient upon reaching the less-wetting/more-wetting discontinuity, and thereafter travels from the less-wetting toward the more-wetting end with a steady speed as long as it bridges the discontinuity.

The basic observable phenomena pertaining to the movement of the slug in the capillary tube have been analyzed, yielding equations for the acceleration and the steady-state speed of the slug as functions of the mass density, surface tension, and viscosity of the liquid; the inner radius and length of the tube; the length of the slug; the orientation of the tube in the gravitational field; and the liquid/tube contact angles in the two differently wetted regions. Experiments have been conducted under conditions intended to minimize the effect of gravitation, using narrow tubes (inner radii of the order of 0.5 mm) oriented horizontally on a table and using wider tubes (inner radii of the order of 5.0 mm) in a drop tower. The results of the experiments agree well with the predictions over a large parametric range. The results also show that the speed is strongly affected by the level of cleanliness of the tube surface.

The technique is expected to prove useful in experiments on the physics of dynamic wetting. Effects of microscopic surface roughness, cleanliness, and patchy wettability could be investigated and quantified in detail. The low-gravity environment of the drop tower affords additional possibilities that could be exploited to enhance understanding of capillary-driven flows on nonideal surfaces.

This work was done by Mark M. Weislogel of Lewis Research Center. Further information is contained in a TSP [see page 1].

Inquiries concerning rights for the commercial use of this invention should be addressed to NASA Lewis Research Center, Commercial Technology Office, Attn: Tech Brief Patent Status, Mail Stop 7–3, 21000 Brookpark Road, Cleveland, Ohio 44135. Refer to LEW-16434.

Capillary-Pumped Loops for Equalizing Body Temperatures

Excess heat from hot regions would be transferred to cold regions.

Goddard Space Flight Center, Greenbelt, Maryland

Capillary-pumped-loop devices are intended for incorporation into protective suits. These thermal-control devices would be used to equalize temperatures for the wearers. For example, a device of this type could be used to transfer excess heat from parts of the human body that tend to become overheated (e.g., armpits) to other parts that tend to become cold (e.g., hands).

A typical device of this type (see figure) would include a capillary evaporator with a wick inside, a condenser, and connecting tubes, all containing a working fluid. The working fluid could be, for example, water, an alcohol, or a non-CFC refrigerant. The wick would be made of a suitable porous material. The wick, the tubes, and the evaporator and condenser housing would have to be made of materials compatible with the working fluid and with each other. Unlike heat pipes, there would be no wicks in the tubes between the evaporator and condenser.

The fluid in liquid form would be held in the wick in the evaporator by capillary action. Absorbing heat from the evapora-

tor surroundings, the fluid would evaporate into channels in the outer surface of the wick. The resulting vapor would flow along these channels to the evaporator outlet, then along a tube to the condenser, the surroundings of which would be cooler than those of the evaporator. The fluid would return to liquid form in the condenser, giving up latent heat of vaporization to the surroundings. The liquid would flow from the condenser, along a return tube to the evaporator inlet. Finally, the liquid would enter the evaporator wick, completing the cycle.

Capillary action in the evaporator should ordinarily provide adequate pump pressure. Optionally, a mechanical pump could be included in case the capillary head provided by the evaporator were insufficient to overcome any frictional head or any static head induced by differences between heights in different parts of the loop. An optional bypass tube could also be included.

There could be many variations on the foregoing basic theme, even apart from the selection of materials. For example:

- Multiple evaporators and/or multiple condensers could be ganged in parallel by use of suitable inlet and outlet manifolds.
- The tubes between the evaporator and condenser could be straight or bent, rigid or flexible, and could have any of a variety of cross-sectional shapes.
- A wick could be installed in the evaporator as well as in the condenser.
- The wick(s) could be fabricated with various combinations of parallel, radial, circular, and/or otherwise patterned interior and/or surface channels to enhance the flows of liquid and vapor.
- The surfaces of the evaporator and condenser could be designed to enhance the transfer of heat.

This work was done by Theodore D. Swanson and Paul Wren (deceased) of **Goddard Space Flight Center.** *Further information is contained in a TSP [see page 1].*

This invention is owned by NASA, and a patent application has been filed. Inquiries concerning nonexclusive or exclusive license for its commercial development should be addressed to the Patent Counsel, Goddard Space Flight Center [see page 1]. Refer to GSC-13329.

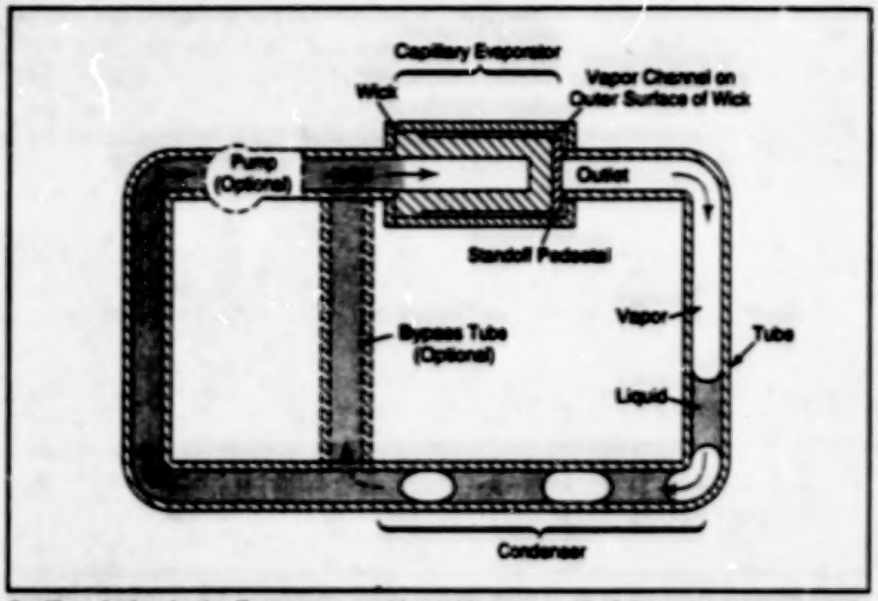

Capillary Action in the Evaporator would provide some or all of the pump pressure needed to circulate the fluid. One of the advantages of capillary pumping is a potential for a low mass-to-heat-transfer ratio.

Image-Warping Coherent Fiber-Optic Bundles

Images could be warped away from nonfunctional areas of retinas to restore some vision.

Lyndon B. Johnson Space Center, Houston, Texas

Tapered coherent fiber-optic bundles of a proposed type would be designed to warp images according to predetermined mappings. In one important potential application, an optical device of this type would be used to compensate partly for the loss of vision in the central part of a retina. The device would warp the image onto the remaining sensitive outer part of the retina, in such a way that a distorted but partly usable version of the central part of the image could be seen.

The distortion of an image onto the remaining functional part of a retina was mentioned as one of the potential applications of a developmental digital/analog image-processing system described in "Programmable Remapper" (MSC-21350), *NASA Tech Briefs*, Vol. 14, No. 6 (June, 1990), page 46. Of course, an image-warping coherent fiber-optic device would lack the programmability of an electronic image-processing system, but in return it would offer ruggedness and essentially unlimited processing speed.

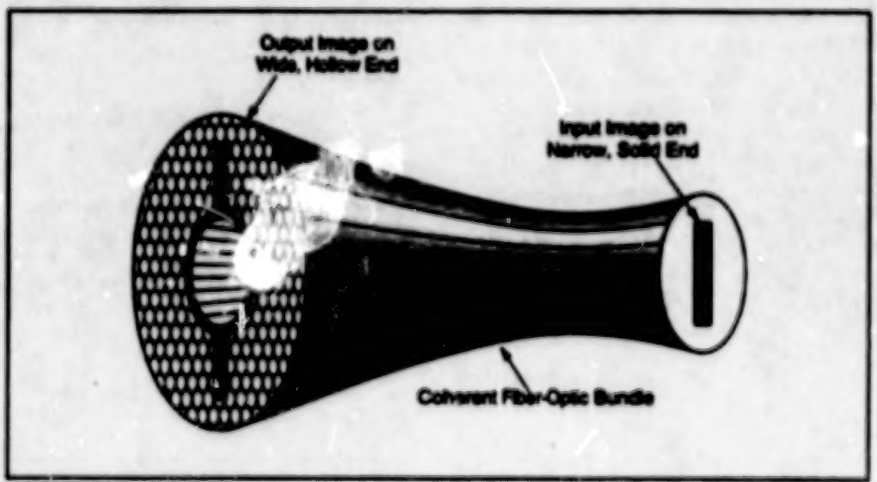

A Coherent Fiber-Optic Bundle would be made to taper from a hollow wide end to a solid narrow end. An image focused on the solid narrow end would emerge from the wider end magnified and warped away from the central region.

Tapered coherent fiber-optic bundles that magnify or minify have been produced by heating and stretching solid,

originally cylindrical coherent fiber-optic bundles. A device of the proposed type would also be made by heating and stretching a cylindrical coherent fiber-optic bundle, but in this case, the bundle would start out as a hollow cylinder; that is, it would have a central hole running along its length. The bundle would be stretched and heated while a vacuum was applied to the central hole (see figure). The atmospheric pressure on the side of the bundle would thus force the sides inward, causing the hole to taper down to a smaller diameter and eventually to close as stretching proceeded. Once the stretched bundle had cooled, a transverse cut would be made at or near the midlength to expose a cross section in which the central hole was closed.

An image focused on the circular surface at the narrow end of the bundle would travel along the optical fibers and would become warped as desired because it would emerge from the corresponding fibers redistributed on the ring surface at the wide end (see figure). No image would be formed in the hollow interior region at the wide end.

This work was done by Richard D. Juday of **Johnson Space Center**. *Further information is contained in a TSP [see page 1].*
MSC-22435

Books and Reports

DLS Sizing of Particles in Hanging Liquid Drops

A report describes an advanced fiber-optic dynamic-light-scattering (DLS) probe and experiments in which the probe was used to measure, noninvasively, the sizes of bovine serum albumin protein molecules and polystyrene latex colloidal particles suspended in small hanging liquid drops. These experiments were performed to verify and demonstrate an emerging capability to use DLS to acquire quantitative information on the nucleation and growth of protein molecules in real time in automated hanging-drop protein-growth apparatuses. DLS is commonly used to characterize macromolecular solutions, but heretofore, DLS instrumentation has been elaborate, with optics that are difficult to align, and has thus not been amenable to *in situ*, real-time monitoring of protein-growth processes. The present developments have been made possible by the miniaturization of solid-state lasers, photodetectors, optical components, and fiber-optic communication devices. The probe demonstrated in the experiments can be operated at a safe level of laser power (≤0.2 mW), features a small scattering volume with a beam diameter of ≈15 μm and high spatial coherence, and enables determination of particle size within an observation time of 5 seconds.

This work was done by Rafat R. Ansari of Case Western Reserve University and Kiweng I. Suh of the National Research Council for **Lewis Research Center**. *To obtain a copy of the report, "Sizing of Colloidal Particles and Protein Molecules in a Hanging Fluid Drop," see TSP's [page 1].*

Inquiries concerning rights for the commercial use of this invention should be addressed to NASA Lewis Research Center, Commercial Technology Office, Attn: Tech Brief Patent Status, Mail Stop 7–3, 21000 Brookpark Road, Cleveland, Ohio 44135. Refer to LEW-16515.

X-Ray-Based Strain Measurements at High Temperatures

A report discusses a method of noncontact extensometry of objects in hot or otherwise hostile environments by use of focusing and scanning of x rays. The method was reported in two previous articles in *NASA Tech Briefs*: "X-Ray Measurements of Displacements in Hostile Environments" (LEW-15905), Vol. 19, No. 6 (June 1995), page 18a and "Progress in X-Ray-Based Displacement and Strain Measurements" (LEW-16001), Vol. 20, No. 10 (October 1996), page 10a. In this method, targets that fluoresce secondary x rays when illuminated by the hard x rays are attached to or embedded in an object to be measured, then a hard-x-ray line image is scanned across the object while fluorescent photons are detected. The fluorescent-photon-counting rate increases or decreases, respectively, as the incident x-ray beam crosses onto or off a target. The position of an edge of the target can be determined from the position of the corresponding change in the photon-counting rate by use of the known scanning geometry. In tests described in the report, the method yielded a repeatability of 0.1 μm for a target on a tensile specimen of Hastelloy-X at temperatures up to 800 °C. A similar degree of repeatability was observed in a room-temperature test of a specimen of a composite of reaction-bonded silicon nitride and silicon carbide.

This work was done by Howard A. Carlstrom, Eric H. Jordan, and Douglas M. Pease of the University of Connecticut for **Lewis Research Center**. *To obtain a copy of the report, "High Resolution X-Ray Based Strain Measurements for Hostile Environments," see TSP's [page 1].*

Inquiries concerning rights for the commercial use of this invention should be addressed to NASA Lewis Research Center, Commercial Technology Office, Attn: Tech Brief Patent Status, Mail Stop 7–3, 21000 Brookpark Road, Cleveland, Ohio 44135. Refer to LEW-16510.

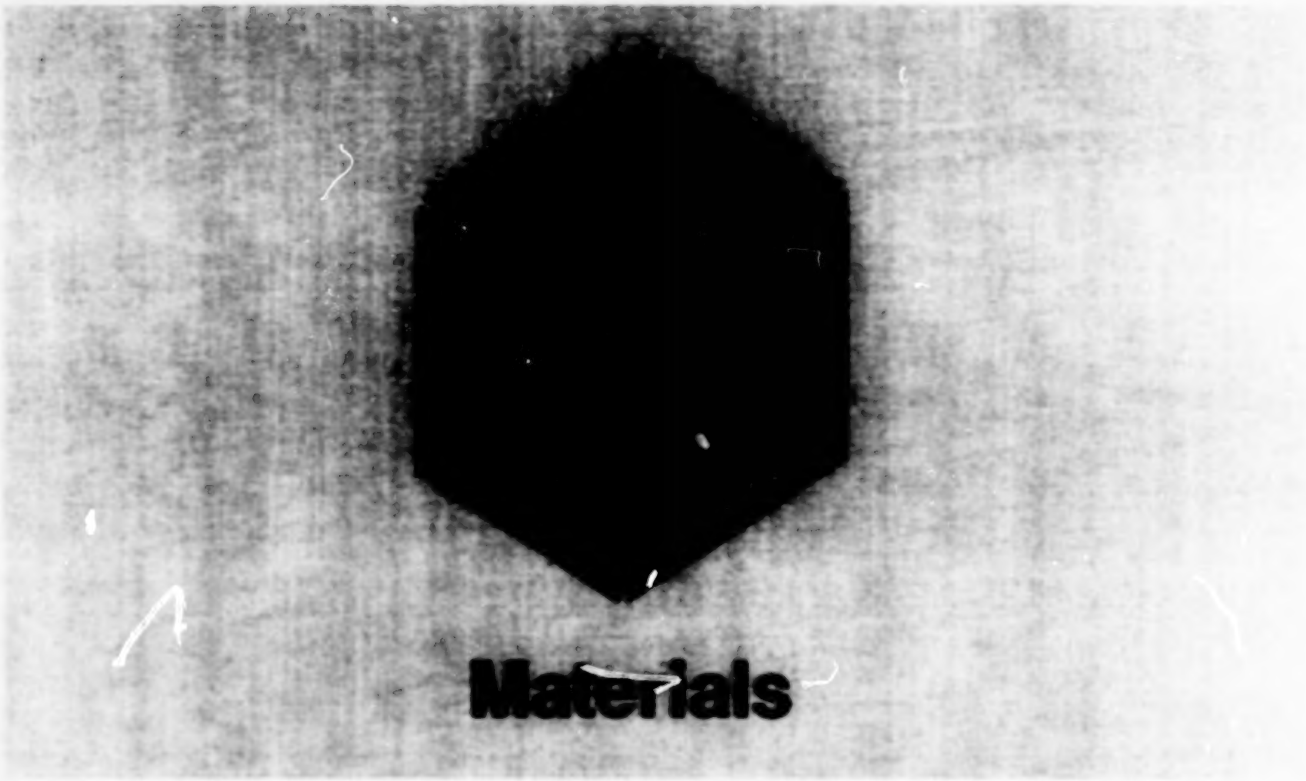

Hardware, Techniques, and Processes

27 Carbon Papers for Negative Electrodes in Lithium Cells
28 Improved Oxidation-Resistant SiC/(Si/SiC) Composites
28 Sputtered Au/C Bilayers as Solid Lubricants on Alumina
29 Lightweight Panels With Embedded Perpendicular Metal Pins
30 Coating Fibers With Ceramics by Use of Slurries
30 High-Strength, Hydrogen-Resistant Alloy

BLANK PAGE

Carbon Papers for Negative Electrodes in Lithium Cells

These papers feature high reversible charge/discharge capacities.

NASA's Jet Propulsion Laboratory, Pasadena, California

Experiments have demonstrated the feasibility of using selected commercial carbon papers as negative electrodes (anodes) of lithium-based electrochemical cells. Various lithium-intercalating materials, including different forms of carbon, are being investigated as candidate anode materials. Li-intercalating materials are attractive as alternative anode materials because, in comparison with lithium itself as the anode material, they offer significant improvements in safety and cycle life.

Some other forms of carbon (including graphite and coke) evaluated for this purpose at NASA's Jet Propulsion Laboratory have thus far proved unsuitable because they have exhibited loss of charge/discharge capacity during the first few charge/discharge cycles. In general, the selection of a carbon Li-anode material is complicated by the strong dependence of charge/discharge characteristics on the specific form of carbon. These characteristics include the intercalation characteristics (amount, kinetics, and potential of Li intercalation), and the loss of capacity (equivalently, the irreversible component of the charge/discharge capacity or "irreversible capacity," for short). The irreversible capacity is consumed during the first few charge/discharge cycles as some of the lithium becomes irreversibly intercalated and surface films form.

Thus, desirable characteristics for a carbon Li-anode material include high reversible capacity at potential close to that of Li at moderate to high rates of intercalation, plus low irreversible capacity. The carbon papers tested in the experiments were found to exhibit such characteristics. These carbon papers are made from carbon fibers of defined history and sources, using binder resins that are eventually carbonized and graphitized. These papers are 60 to 80 percent porous, and, in comparison with some other forms of carbon, are flexurally strong and highly electrically conductive. The carbon papers are available with various fiber lengths and in various thicknesses. They are used commercially in several applications, including fuel cells and supercapacitors.

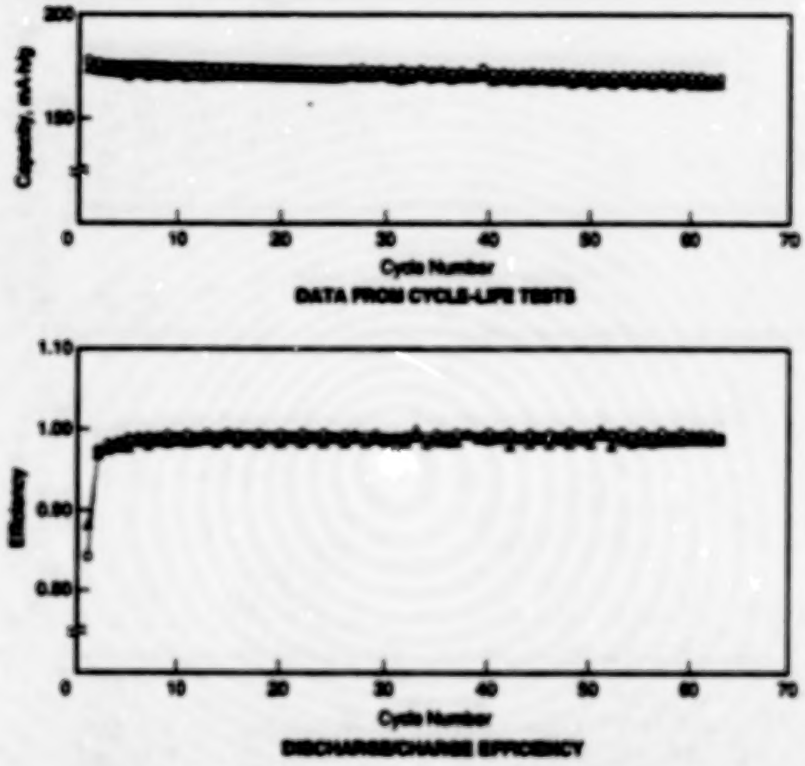

Data From Charge/Discharge Cycling Tests of Li cells containing anodes made from two commercial carbon papers illustrate the high performances achievable when these papers are used as alternatives to lithium itself as the anode material.

In the experiments, sheets of the carbon papers were electrochemically tested against $LiCoO_2$ cathode in an electrolyte solution that comprised $LiPF_6$ dissolved in a mixture of ethylene carbonate and diethyl carbonate. A lithium reference electrode was included in each electrochemical cell. Microporous polypropylene sheets were used as electrode separators, and polytetrafluoroethylene shims were used to provide compaction for the electrode stack. The cell was subjected to charge/discharge cycles by use of an automatic battery cycler at a constant current density of 0.2 mA/cm^2, between cutoff potentials of 4.1 V on charge and 2.5 V on discharge.

As shown in the upper part of the figure, the measured charge/discharge capacities started high and remained high after 65 cycles (tests were continuing when the information was submitted for this article). The lower part of the figure presents the measured values of discharge/charge efficiency, which is defined as the ratio between the capacity during a given discharge and the capacity during the immediately preceding charge; this plot shows that within the first few cycles, each cell achieved a discharge/charge efficiency close to 100 percent. Both carbon papers were found to exhibit relatively high (≈ 175 mAh/g) reversible Li-intercalation capacities, with a relatively low (≈ 40 mAh/g) irreversible capacity. These performance characteristics are comparable or superior to the majority of other carbon/graphite materials, and the carbon papers can be easily tailored to satisfy specific needs.

This work was done by Ratnakumar V. Bugga, Chen-Kuo Huang, Subbarao Surampudi, and Gerald Halpert of Caltech for **NASA's Jet Propulsion Laboratory**. *Further information is contained in a TSP [see page 1].*

NPO-19503

Improved Oxidation-Resistant SiC/(Si/SiC) Composites

Matrix additives and fiber coatings help to seal cracks to retard infiltration of oxygen.

Lewis Research Center, Cleveland, Ohio

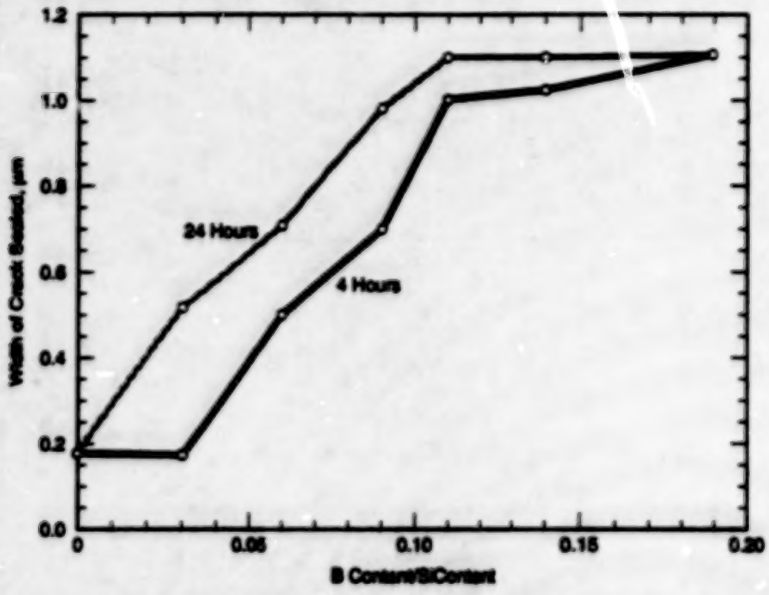

The Widths of Cracks That Were Sealed were measured in SiC/(Si/SiC) specimens that contained various proportions of boron. The specimens were exposed, variously, for 4 or 24 hours, to an atmosphere of 90 percent water and 10 percent oxygen at a temperature of 900 °C.

Improved composites of SiC fibers in Si/SiC matrices have been invented for use in applications in which there are requirements for materials that can resist oxidation at high temperatures in the presence of air and steam. Such applications are likely to include advanced aircraft engines and gas turbines.

The need for the improved composites arises as follows: Although both the matrix and fiber components of older SiC/(Si/SiC) composites generally exhibit acceptably high resistance to oxidation, these composites become increasingly vulnerable to oxidation and consequent embrittlement whenever mechanical or thermomechanical loads become large enough to crack the matrices. Even the narrowest cracks become pathways for the diffusion of oxygen.

Typically, to impart toughness to an SiC/(Si/SiC) composite, the SiC fibers are coated with a material that yields at high stress to allow some slippage between the fibers and matrix. If oxygen infiltrates through the cracks to the fiber coatings, then, at high temperature, the oxygen reacts with the coatings (and eventually with the fibers), causing undesired local bonding between fibers and the matrix and consequent loss of toughness. In addition, the resultant concentration of stress and deterioration of the fibers at the bonding locations give rise to failure of fibers. If the process of infiltration and oxidation continues, then eventually the remaining fibers become unable to bear the load, causing the composite to fail at a stress appreciably below its initial (as-fabricated) ultimate strength.

The improved composites incorporate matrix additives and fiber coatings that retard the infiltration of oxygen by reacting with oxygen in such a way as to seal cracks and fiber/matrix interfaces at high temperatures. These matrix additives and coating materials contain glass-forming elements — for example, boron (see figure) and germanium.

Boron is particularly suitable for use in fiber coatings because it can react with oxygen to form boron oxide, which can, in turn, interact with the silica formed by oxidation of the matrix and fiber materials to produce borosilicate glasses. Boron and SiB_6 may prove to be the coating materials of choice because they do not introduce any elements beyond those needed to form borosilicate glasses.

One way to fabricate an SiC/(Si/SiC) composite object is to first make a preform of silicon carbide fibers interspersed with a mixture of silicon carbide and carbon particles, then infiltrate the preform with molten silicon. Boron can be incorporated by chemical vapor deposition onto the fibers prior to making the preform.

Boron and germanium can be incorporated into the matrix by adding these elements to either the matrix or the molten silicon infiltrant. Inasmuch as the solubility of boron in silicon is limited, it may be necessary to add the boron via the preform in a typical case.

This work was done by F. N. Mazandarany of General Electric Co. for **Lewis Research Center**. *Further information is contained in a TSP [see page 1].*

Inquiries concerning rights for the commercial use of this invention should be addressed to NASA Lewis Research Center, Commercial Technology Office, Attn: Tech Brief Patent Status, Mail Stop 7–3, 21000 Brookpark Road, Cleveland, Ohio 44135. Refer to LEW-16386.

Sputtered Au/Cr Bilayers as Solid Lubricants on Alumina

Friction and wear in slow sliding at high temperatures are reduced.

Lewis Research Center, Cleveland, Ohio

Sputter-deposited surface bilayers of gold on chromium have been found to be effective as solid lubricants to protect alumina substrates in applications that involve sliding at high temperatures. The use of thin surface layers of gold, lead, copper, or other soft metals to protect hard metallic substrates is well known. Whether the substrate is metal or, as in this case, ceramic, the basic principle of solid lubrication remains the same: under a sliding load, the soft overlayer (in this case, gold) shears rather than abrades, and thereby protects the hard substrate, which carries the mechanical load.

The novel aspect of the present development lies in the particular choice of materials, which was guided by the

following considerations:

- The low thermal conductivity and high thermal stability of alumina make it an attractive candidate substrate material for high-temperature applications.
- Gold offers the advantages of chemical stability and a relatively high melting temperature of 1,073 °C.
- Unfortunately, because of its chemical stability (nonreactivity), gold adheres poorly to alumina substrates; gold does not even wet alumina. This makes it necessary to deposit an interlayer of a more reactive metal between the alumina substrate and the gold overlayer so that the gold overlayer can adhere.
- Chromium has been used in the electronics industry to form bonding interlayers between silicon substrates and gold surface electrical contacts.

The concept of sputter-deposited Au/Cr coatings as solid lubricants was tested in experiments in a high-temperature pin-on-disk tribometer. Alumina disks — some uncoated and others sputter-coated Au/Cr bilayers — were slid against uncoated alumina pins in air at temperatures from 25 to 1,000 °C, at sliding speeds from 1 to 15 m/s, and with pins pressed against disks at various loads from 4.9 to 49 N. Friction forces were measured during the tests, and post-test analyses were performed to determine the nature and extent of wear.

The results of the experiments (for example, see figure) indicate that in the presence of Au/Cr surface layers, friction was reduced by about half. In most cases, the coefficients of friction of Au/Cr-coated specimens decreased with temperature from 25 to 1,000 °C. At the lowest sliding speed of 1 m/s, pin-wear factors [wear volume ÷ (load force × sliding distance)] for Au/Cr-coated disks were found to be 10 to 100 times lower than for uncoated disks. Pin-wear factors were largely unaffected by increasing loads up to 29.4 N. Sliding speed had little effect on friction. However, wear factors for Au/Cr-coated specimens increased strongly with sliding speed, even exceeding those for uncoated specimens in some cases. On the basis of these results, it appears that Au/Cr coatings provide adequate lubrication for moderately loaded sliding alumina substrates at speeds up to about 1 m/s and temperatures up to 1,000 °C.

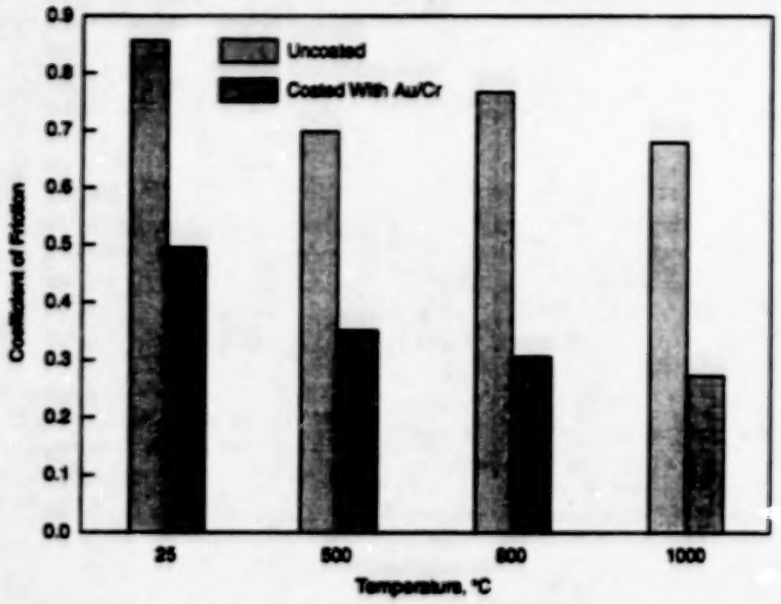

These Coefficients of Friction were determined from experiments with uncoated and Au/Cr-coated alumina disks at a sliding speed of 1 m/s and a pin/disk load force of 4.9 N.

This work was done by Christopher DellaCorte of **Lewis Research Center** *and Patricia A. Benoy of Saint Louis University. Further information is contained in a TSP [see page 1].*

Inquiries concerning rights for the commercial use of this invention should be addressed to NASA Lewis Research Center, Commercial Technology Office, Attn: Tech Brief Patent Status, Mail Stop 7–3, 21000 Brookpark Road, Cleveland, Ohio 44135. Refer to LEW-16467.

Lightweight Panels With Embedded Perpendicular Metal Pins

These panels have potential for both terrestrial and outer-space applications.

Marshall Space Flight Center, Alabama

Lightweight panels made of organic composite materials with embedded metal pins oriented through the thickness (see figure) have been investigated for their potential utility as the outer layers of multilayer shields ("bumpers") to protect spacecraft against high-speed impacts of natural and artificial debris. Composite-material panels containing through-thickness pins are also of great potential use on Earth; for example, composite panels with pins embedded using this manufacturing technique have been shown to yield a twenty-fold increase in delamination resistance, when compared with the same composite without pins, resulting in significantly improved composite aircraft structures. Similarly, this approach has great potential appeal for the joining of composite components, such as skin panels to supporting ribs. In addition, the use of embedded pins can increase the through-thickness thermal conductivity of panels, making them potential candidates for electronic-packaging support structures.

In the spacecraft application, an outer bumper panel would be used to fragment debris particles incident at speeds of the order of 3 km/s. The fragmented debris would be further fragmented and spread out by an inner bumper panel (typically made of aluminum) before reaching the pressure wall of the spacecraft. Thus, the impact of each debris particle would be spread over a large area of the spacecraft structure to minimize damage to the pressure wall. The protective function of the pins is to provide high shock impedance to promote fragmentation of incident debris. The function is essentially

the same (albeit in a reversed role) as that of long-rod penetrators that have been used on Earth to defeat tank armor. In experiments in which high-speed projectiles with masses of the order of 1 g were used to simulate incident space debris, pins with diameters of 7.5 mils (0.19 mm) embedded in graphite-fiber/epoxy-matrix composite at a volume fraction of 4 percent provided better protection than did pins of greater diameter or pins embedded at smaller volume fractions. More importantly, in a hypervelocity test at normal incidence, a double bumper having a composite front layer containing embedded pins and a spaced rear layer of aluminum significantly outperformed a similar bumper in which both layers were made of aluminum.

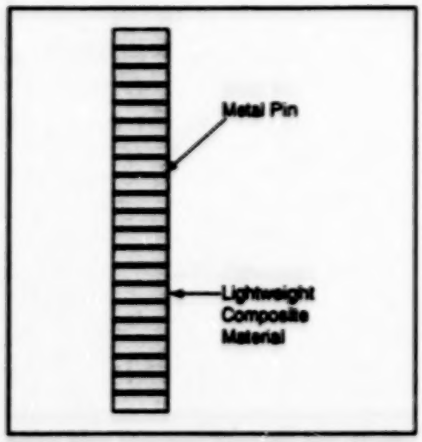

Metal Pins Oriented Through the Thickness of a lightweight composite-material panel impart special mechanical and thermal characteristics, depending on the pin material, diameter, and volume fraction.

Of course, for terrestrial applications, it is often preferable to use pins of different materials, diameters, and volume fractions. The process has considerable flexibility, and composite panels have been made successfully using pins of various types of metals as well as nonmetals.

This work was done by John Gassner, Patricia Schwartz, and Charles Carey of Foster-Miller, Inc., for **Marshall Space Flight Center**. *Further information is contained in a TSP [see page 1].*

Inquiries concerning rights for the commercial use of this invention should be addressed to the Patent Counsel, Marshall Space Flight Center [see page 1]. Refer to MFS-26368.

Coating Fibers With Ceramics by Use of Slurries

This method is an attractive alternative to chemical vapor deposition.

Lewis Research Center, Cleveland, Ohio

Fibers for use in metal-matrix/fiber composite materials can be coated with ceramic-matrix/fiber interfacial layers by use of slurries. Heretofore, it has been common practice to form these interfacial layers by chemical vapor deposition (CVD). The slurry coating method offers several advantages over CVD — including lower cost.

CVD entails a number of disadvantages:

- Coating the fibers by CVD is very costly because of the capital equipment involved and because special tooling is usually needed.
- CVD adds a separate step to the overall process of fabrication of a metal-matrix/fiber composite.
- Coatings formed by CVD are susceptible to damage from handling.
- In an application in which fibers are required to be woven, coating must be done after weaving, and this generally necessitates an additional desizing operation.

In the slurry method, an ultrafine (particle sizes < 1 μm) ceramic powder is dispersed in a typical fiber-sizing solution, which could be polyvinyl acetate, for example. The formulation of this slurry is such as to achieve (1) a stable colloidal suspension of the ceramic particles and (2) a viscosity appropriate for fiber sizing. The suspension can also include dispersing and/or deflocculating agents and/or surface-wetting agents.

The principal advantage and novel aspect of this slurry method is that the fibers can be coated during the sizing step of the fiber-manufacturing process. Therefore, the fibers can be coated in a more nearly pristine state, and the combination of the coating and sizing affords some protection for both the fibers and the coating against damage from handling in subsequent operations. Thus, fibers could be woven in the coated state if necessary, and the sizing compound could be burned off prior to infiltration of the woven fabric with matrix material.

The low cost (relative to CVD) of this slurry coating method is realized directly through reduction in the number of processing steps, lower prices of raw materials, and less use of expensive capital equipment. Part of the reduction in cost is realized indirectly through the processing flexibility that results from increased ease of handling of the coated fibers and the possibility of weaving fibers in the coated state.

This work was done by Stuart A. Sanders and Imelda P. Smyth of United Technologies for **Lewis Research Center**. *No further documentation is available.*

Inquiries concerning rights for the commercial use of this invention should be addressed to NASA Lewis Research Center, Commercial Technology Office, Attn: Tech Brief Patent Status, Mail Stop 7-3, 21000 Brookpark Road, Cleveland, Ohio 44135. Refer to LEW-16060.

High-Strength, Hydrogen-Resistant Alloy

Innovative new alloy can be readily fabricated into components suitable for use in hydrogen environments.

Marshall Space Flight Center, Alabama

NASA-23 is a hydrogen-resistant alloy that has been developed for applications in which there are requirements for high strength and high resistance to corrosion. The technology for this alloy was spurred by the fact that the industry did not have high-strength, hydrogen-resistant alloys available.

Adequate resistance to corrosion is necessary for the survival of alloys in hydrogen environments. Alloys for use in such environments typically contain a minimum of

10 weight percent chromium. The unique feature of NASA-23 is that it combines high strength with resistance to corrosion, and can readily be made into parts that are suitable for use in hydrogen environments.

The use of high-strength alloys that have low resistance to hydrogen results in frequent replacement of components because hydrogen severely degrades mechanical properties of these alloys. At present, coatings that serve as barriers to hydrogen/metal interactions are often applied to such alloys used in hydrogen. However, the use of coatings does result in higher production costs. Additionally, alloys that have lower resistance to hydrogen can be used by increasing section sizes; however, this method results in an increase in component weight.

NASA-23 can be used for components that encounter temperatures up to 1,200 °F (649 °C) in hydrogen environments.

Innovators of NASA-23 carefully chose alloying elements of iron, nickel, cobalt, chromium, niobium, titanium, and aluminum to ensure adequate precipitation hardening for strength and minimum precipitation of detrimental grain boundary precipitates.

This work was done by B.N. Bhat and W. B. McPherson of the **Marshall Space Flight Center** *and A.K. Kuruvilla of IITRI. Further information is contained in a TSP [see page 1].*
MFS-26493

BLANK PAGE

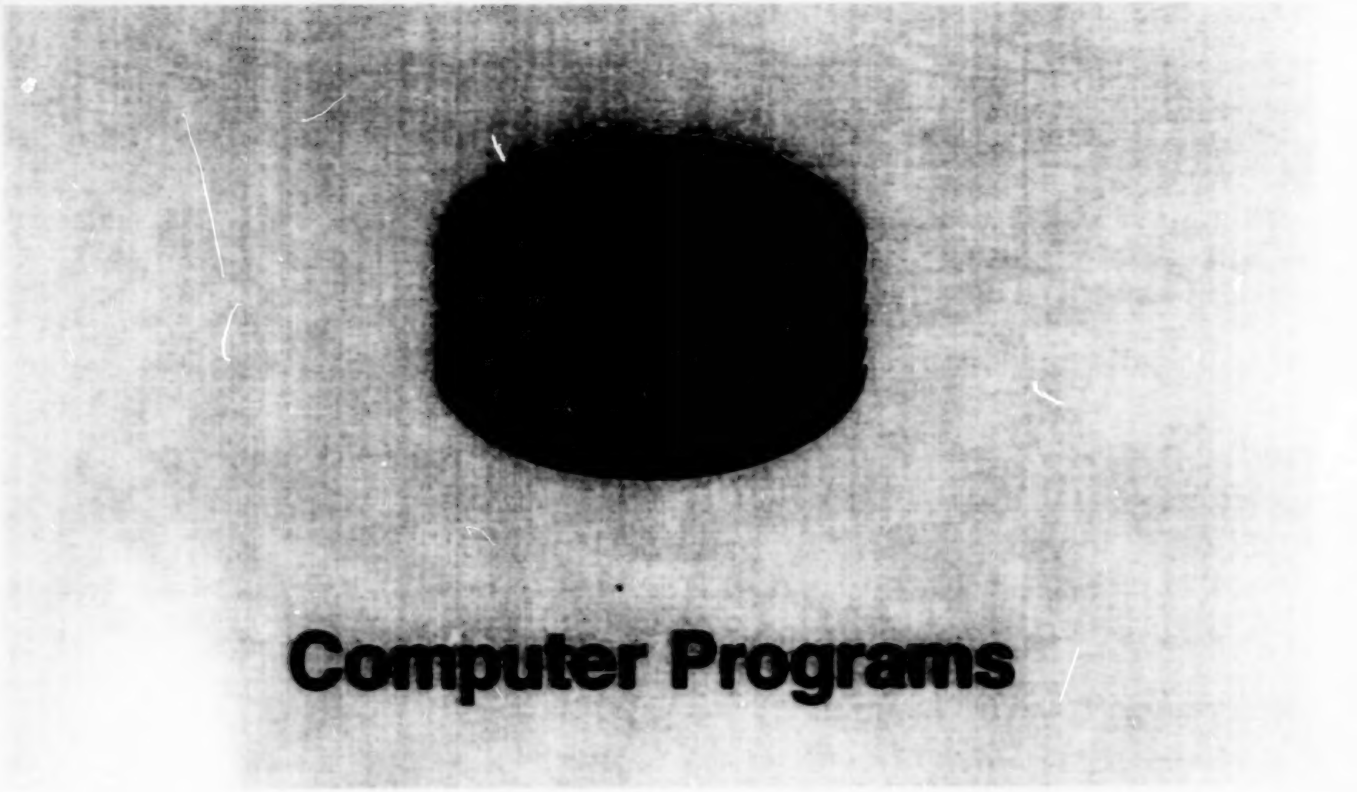

Computer Programs

Physical Sciences

35 Predicting Performance of a Nickel/Cadmium Power Cell
35 Software for Modeling Dynamics of Optical Interferometers
35 Improved Software for Modeling Controlled Optical Systems

Mathematics and Information Sciences

35 Algorithm for Lossy/Progressive/Lossless Image Compression
36 Prototype Distributed-Visualization Software System
36 Optimizing Program Does Feasible-Directions Gradient Search
36 Software for Automating the Design-Optimization Process
37 Software Helps Determine Viability of New Products
37 Program for Remote Viewing of Reports Containing Graphics

BLANK PAGE

Computer Programs

Programs with no telephone numbers listed may be available from:

COSMIC®
Computer Services Annex
University of Georgia
Athens, GA 30602
Telephone No. (404) 542-3265.

Physical Sciences

Predicting Performance of a Nickel/Cadmium Power Cell

The Nickel Cadmium Performance Prediction Model computer program predicts the current, voltage, heating, efficiency, state of charge, and other parameters that characterize the performance of a nickel/cadmium electrochemical cell. This program could be used in the design and operation of Ni/Cd batteries, products that contain Ni/Cd batteries, and chargers for Ni/Cd batteries. The program implements a mathematical model based on first principles; it includes submodels of thermodynamics, mass transport, chemical kinetics, mass balance, and energy balance. Kinetic equations for eleven different reactions (including solid/liquid and gas-phase reactions) are included. Unlike other Ni/Cd-performance-predicting programs driven by static data bases or analog circuit models, this program is capable of predicting time-dependent and hysteretic behavior. This program is easy to use, and can be executed on any Apple Macintosh or compatible computer. To be able to run a graphical user interface in the program, one must use the AppleScript and MacOS 7.5 software. The program requires less than 4 MB of disk storage (including user files) and only 4 MB of random-access memory.

This program was written by Paul J. Timmerman and Carlos E. Sanchez of Caltech for **NASA's Jet Propulsion Laboratory**. *Further information is contained in a TSP [see page 1].*

This software is available for commercial licensing. Please contact Don Hart of the California Institute of Technology at (818) 393-3425. Refer to NPO-19991.

Software for Modeling Dynamics of Optical Interferometers

The Single Mode Acquisition Code (SMAC) computer program mathematically models the optical, mechanical, and electronic dynamics of high-finesse, long-baseline, multiple-cavity optical interferometers like those used in gravity-wave detectors. Dynamical situations that can be simulated include those that involve noise and/or multiple modulation frequencies and sidebands. SMAC includes components for modeling the dynamics of cavity-control servomechanisms, electronic closed-loop servo control subsystems, and synchronous-detection electronic circuitry. Nonlinear time-domain models are incorporated for use in designing and testing lock-acquisition controllers. Once lock has been achieved, small-amplitude transfer functions represent cavity signals adequately. SMAC provides a graphical user interface for defining problems and controlling execution with respect to the problems. SMAC also provides extensive pre- and post-processing support.

This program was written by Laura Needels, David Redding, and Lisa Sievers of Caltech for **NASA's Jet Propulsion Laboratory**. *Further information is contained in a TSP [see page 1].*

This software is available for commercial licensing. Please contact Don Hart of the California Institute of Technology at (818) 393-3425. Refer to NPO-20122.

Improved Software for Modeling Controlled Optical Systems

Modeling and Analysis for Controlled Optical Systems (MACOS) is an easy-to-use computer program for simulating and analyzing the behaviors of a variety of optical systems. MACOS includes S-MACOS, a subroutine software package that provides MACOS commands to any program written by the user, enabling the incorporation of full optics-modeling functionality into other computer codes. MACOS and S-MACOS are improved versions of COMP and SCOMP, which have been applied to more than 30 space- and ground-based instrument systems, including telescopes, cameras, radio antennas, optical interferometers, imaging spectrographs, integrated optical devices, and adaptive-optics systems. MACOS features include a command-line user interface, graphical display of results, interactive dialogues that guide the user through all functions, and ten levels of macros. System models are built up from component models of optical elements (e.g., mirrors, lenses, and diffraction gratings) and surface types (e.g., flats and conics of revolution). Instrument-simulation capabilities are achieved through hybrid ray-trace and physical-optics diffracted-beam propagation combined with sophisticated imaging simulation features. MACOS includes such unique integrated modeling features as linear matrix models of optical instruments and the ability to export linear models directly into Matlab or other numerical-analysis software environments for integration into system-level analyses.

This program was written by David C. Redding and Laura Needels of Caltech for **NASA's Jet Propulsion Laboratory**. *Further information is contained in a TSP [see page 1].*

In accordance with Public Law 96-517, the contractor has elected to retain title to this invention. Inquiries concerning rights for its commercial use should be addressed to

Technology Reporting Office
JPL
Mail Stop 122-116
4800 Oak Grove Drive
Pasadena, CA 91109
(818) 354-2240

Refer to NPO-19841, volume and number of this NASA Tech Briefs *issue, and the page number.*

Mathematics and Information Sciences

Algorithm for Lossy/Progressive/Lossless Image Compression

The Efficient Reversible Image Compression (ERIC) algorithm compresses and decompresses image data at selectable

performance levels. By use of a fast integer wavelet transform, the algorithm losslessly compresses the data on an image into several subimages that represent the image at various levels of spatial resolution and amplitude accuracy. Each subimage is then entropy (Huffman) coded. Decompression of the first subimage reconstructs the image data at the lowest level of accuracy. Decompression of subsequent subimages reconstructs the image data at progressively greater accuracy. Decompression of all subimages reconstructs the original image data exactly. Inasmuch as less-accurate approximations require less data-transmission bandwidth, the algorithm is particularly useful where the user finds it necessary to choose the closest approximation achievable under a given bandwidth constraint. The lossless-compression ratios achieved by this algorithm exceed those of the best previously available standard lossless compression algorithms, which do not give progressively accurate approximations.

This program was written by Eric Majani of Caltech for **NASA's Jet Propulsion Laboratory.** *Further information is contained in a TSP [see page 1].*

This software is available for commercial licensing. Please contact Don Hart of the California Institute of Technology at (818) 393-3425. Refer to NPO-20141.

Prototype Distributed-Visualization Software System

An image-distribution system was developed to facilitate interactive manipulation of high-data-volume images by remote users over a slow network. The system is based on a client/server model integrating a high-performance server running parallel visualization applications and a remote client workstation providing control and display. In order to deliver the image frames generated by the visualization server to the client system quickly, the image distribution system employs a data-compression algorithm developed at JPL, ERIC (Efficient Reversible Image Compression), to reduce the data volume.

The software system employs various optimization steps to provide greater than 5 video frames per second at the client system. The optimization steps include pipelining of the compression, transmission, and decompression and the use of shared-memory X calls. The pipelining minimizes the compression process overhead by balancing the execution times involved in compression, transmission, and decompression and by overlapping these steps.

In this system, compression can be performed in either lossy mode or lossless mode. The lossy mode, is used for quick browse where the data quality is not as important or for applications with a preset data quality. The lossless mode is used where data quality may be important but cannot be set a priority. In this mode, the data can be sent progressively until the quality has been satisfied up to the original quality.

The server system with an API is available on a Cray T3D and it can be integrated with parallel visualization applications producing monochrome image as well as multispectral images. A demonstration system was developed integrating an interactive parallel volume renderer at Cray Research Center in Minnesota and an SGI Indigo 2 workstation at JPL in California. It was successfully demonstrated, displaying 5 monochrome image frames per second on the SGI.

This program was written by Roberto Mendoza, Eric Majani, and Meemong Lee of Caltech for **NASA's Jet Propulsion Laboratory.** *Further information is contained in a TSP [see page 1].*

This software is available for commercial licensing. Please contact Don Hart of the California Institute of Technology at (818) 393-3425. Refer to NPO-20137.

Optimizing Program Does Feasible-Directions Gradient Search

Interactive software guides the user in solving design-optimization problems.

SEEK is a general-purpose optimizing software tool that performs a gradient search optimization of the user's problem to find a best set of design parameters. SEEK was written to assist a mechanical designer in developing a balanced optimal design, keeping the designer in the process while searching systematically among potential designs.

SEEK was also written to be interactive and to communicate clearly to the user. It requires the user to write two analysis subroutines and an input data file for his/her application. By requiring text labels for all variables, the program is able to label its restatement of the problem and all results in the user's words. Optimization is performed by use of a modified feasible-directions gradient technique. The SEEK output file includes an echo of the input data and an analysis of the optimized design. In addition to finding its own optimum, the program allows the user to enter alternative designs for comparative analysis. Analyses of all user designs are also included in the output file.

The SEEK user's manual illustrates the model preparation and programming required to use SEEK for four examples: a bushing design, a spring design, a gear design, and a curve fit. Each of these examples represents a different design problem. The use of SEEK is limited to solving problems that can be modeled continuously with finite constraint and objective-function values over the search area.

SEEK is written in FORTRAN 77 for use on IBM PC-series and compatible computers running MS-DOS. A FORTRAN 77 compiler is required. SEEK has been successfully implemented on an IBM PC 486DX/33 computer running MS-DOS 5.0 with the Lahey F77L 5.1 compiler. The standard distribution medium for SEEK is one 3.5-in. (8.89-cm), 1.44MB, MS-DOS-format diskette. SEEK was released to COSMIC in 1997 and is a copyrighted work with all copyright vested in NASA.

This program was written by Harold H. Coe of **Lewis Research Center** *and M. Savage of the University of Akron. Further information is contained in a TSP [see page 1].*
LEW-16446

Software for Automating the Design-Optimization Process

The Optimization Assistant (OASIS) computer program is a research prototype of a design-optimization software tool. It is being developed to automate much of the process of solving a complex constrained optimization problem of the type encountered in designing a spacecraft, and to facilitate rapid "what-if" analysis of design. As currently envisioned, OASIS would comprise three major components: (1) a set of generic, configurable, metaheuristic optimization algorithms (including genetic and simulated-annealing algorithms); (2) an adaptive problem solver based on artificial-intelligence and machine learning techniques; and (3) a spacecraft-design model. For a given design-optimization problem, the spacecraft-design model would accept, as input, the decision variables to be optimized and would output the value of an objective function. For the specific problem, the adaptive problem solver would select an appropriate optimization algorithm and configure it, minimizing the

need for intervention by the user to customize software for that problem.

This program was written by Alex Fukunaga, Steve Chien, and Andre Stechert of Caltech for **NASA's Jet Propulsion Laboratory**. *Further information is contained in a TSP [see page 1].*

This software is available for commercial licensing. Please contact Don Hart of the California Institute of Technology at (818) 393-3425. Refer to NPO-20073.

Software Helps Determine Viability of New Products

The Product Survey Tool computer program facilitates the collection and analysis of data for predicting the viability of a new system, product, or project (hereafter, "product" for short), while the product has not yet advanced beyond the concept stage. The program asks questions about the product and, through a graphical user interface, collects the answers. The program stores the answers in a database, from which the answers can be extracted and summarized or plotted to assist managers in making decisions about viability. The program has been partially developed, and some of the questions are specific to the original application at Kennedy Space Center. Further developments in the areas of report generation, graphical display of results, maintenance optimization, and data security are needed to fully realize the commercial potential.

This work was done by Charles L. Wood and Curtis C. Dugger of **Kennedy Space Center**. *Further information is contained in a TSP [see page 1].*

Inquiries concerning rights for the commercial use of this invention should be addressed to the Patent Counsel, Kennedy Space Center [see page 1]. Refer to KSC-11925.

Program for Remote Viewing of Reports Containing Graphics

The On-line Report Viewing Application computer program provides a graphical user interface for displaying the contents of management-presentation-style reports that contain mostly charts and graphs. The program makes it unnecessary to print and mail multiple copies of the reports. Residing on a mainframe computer where the original electronic copies of the reports are maintained, the program enables readers to gain access to the reports through their individual computer workstations in a network connected to the mainframe computer. Maintaining the original electronic copies of the reports on the mainframe computer offers an additional advantage of rapid, semiautomatic updating of the reports. Access to reports is limited to authorized readers by use of identification codes. The application also tracks user access down to user ID for management visibility of the usefulness of the report. An authorized reader can use a mouse to move through a report and/or select a specific page, chart, or graph by name. The reader can also print any page of the report.

This work was done by Thomas C. Woodbridge of United Space Alliance (formerly Lockheed Martin) for **Kennedy Space Center**. *Further information is contained in a TSP [see page 1].*

Inquiries concerning rights for the commercial use of this invention should be addressed to the Patent Counsel, Kennedy Space Center [see page 1]. Refer to KSC-11896.

BLANK PAGE

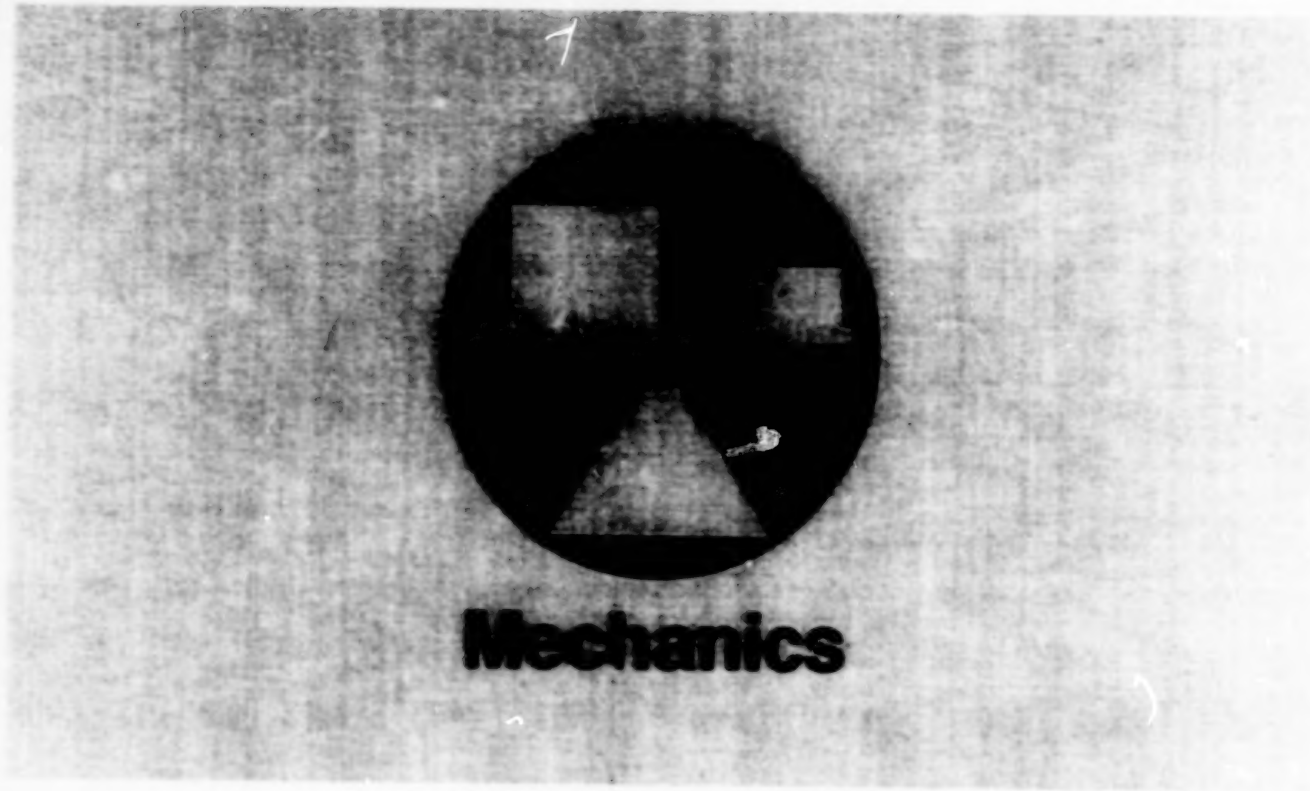

Hardware, Techniques, and Processes

41 Solenoid Valve Modified To Prevent Leakage During Vibration
41 Digital Particle-Image Velocimetry Enhanced by Fuzzy Logic

BLANK PAGE

Solenoid Valve Modified To Prevent Leakage During Vibration

An armature is redesigned, and a spring is added.

Lewis Research Center, Cleveland, Ohio

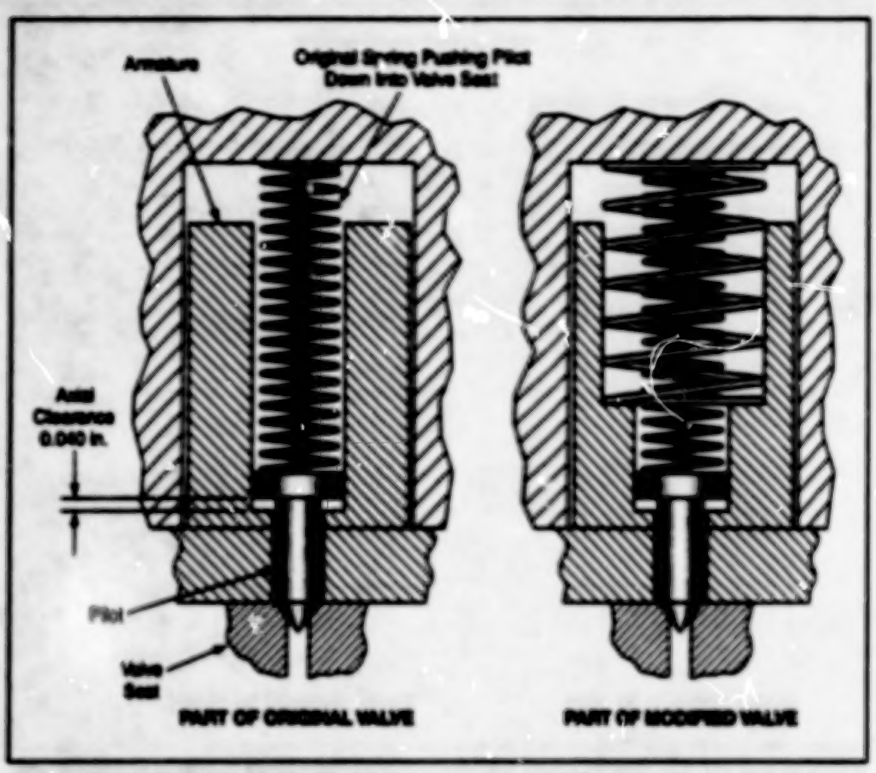

The Additional Spring in the Modified Valve pushes the armature down with just enough force to prevent chatter within the axial clearance. This figure presents a simplified view to illustrate the basic principle of the modification; the actual design is somewhat more complex.

A solenoid valve has been modified to suppress chatter, which made the valve susceptible to leakage in a vibratory environment. In the original design, an axial clearance of 0.040 in. (1 mm) between the armature and the pilot (see figure) left the armature free to chatter. Sometimes, the chatter knocked the pilot out of the valve seat, thereby causing leakage. Even though the pilot and seat were configured for pressure-assisted seating, a differential pressure across the valve seat of 1,800 psi (12 MPa) was insufficient to prevent leakage during vibration of the valve.

Elimination of the armature/pilot clearance was not an option because during normal operation, the clearance is utilized to develop momentum of the armature for a hammering effect that assists in opening the valve; with the help of the hammering effect, the valve can be opened at a differential pressure up to the rated value of 2,500 psi (17 MPa). Installation of a stiffer spring pushing down on the pilot from inside the armature was also not an option because it would reduce the maximum opening differential pressure below the rated value.

The modification that was finally chosen was one that eliminated chatter while not impairing the ability of the valve to open at the rated differential pressure. The original armature was replaced by a new armature containing an additional counterbore wider than the original counterbore. The new counterbore accepts a spring that has a diameter greater than that of the original spring and that surrounds the original spring. The original spring is retained and is still used to push the pilot down into the valve seat. The new spring pushes the armature down with just enough force to prevent chatter during vibration.

This work was done by Michael W. Henry of Aerospace Design & Fabrication, Inc., for Lewis Research Center. Further information is contained in a TSP [see page 1].

Inquiries concerning rights for the commercial use of this invention should be addressed to NASA Lewis Research Center, Commercial Technology Office, Attn: Tech Brief Patent Status, Mail Stop 7–3, 21000 Brookpark Road, Cleveland, Ohio 44135. Refer to LEW-16344.

Digital Particle-Image Velocimetry Enhanced by Fuzzy Logic

Particle velocities can be measured with high spatial resolution over a broad range of seeding densities.

Lewis Research Center, Cleveland, Ohio

A method of digital particle-image velocimetry (digital PIV) involves the use of a combination of fuzzy-logic, cross-correlation, and particle-tracking techniques. As in other PIV methods, the overall task is to estimate the velocity field in one plane of a flowing gas or liquid by (1) seeding the flow with small, highly reflective particles, (2) illuminating the plane of interest with intense light from a pulsed laser or other source, (3) recording a sequence of images of the illuminated particles (see figure), and (4) processing the image data to determine local velocity vectors from displacements of particle images. Older PIV methods described previously in *NASA Tech Briefs* involve various degrees of manual and/or automated processing of image data by hardware and/or software. The present method is a product of a continuing effort to develop a capability for all-electronic, fully automated, software-based processing of digitized seed-particle images to extract the maximum available information about velocities.

In the present method, the same scene is both illuminated by two pulsed lasers via a beam combiner and observed by two charge-coupled-device cameras via a beam splitter. Each camera acquires a single-exposure image. The reason for using two cameras and two lasers is simply to make it possible to record the two images as close together or as far apart in time as necessary to obtain particle-image displacements in the right size range for extraction of velocity data.

The image data are then analyzed in a two-stage process. In the first stage, the images from the two cameras are divided

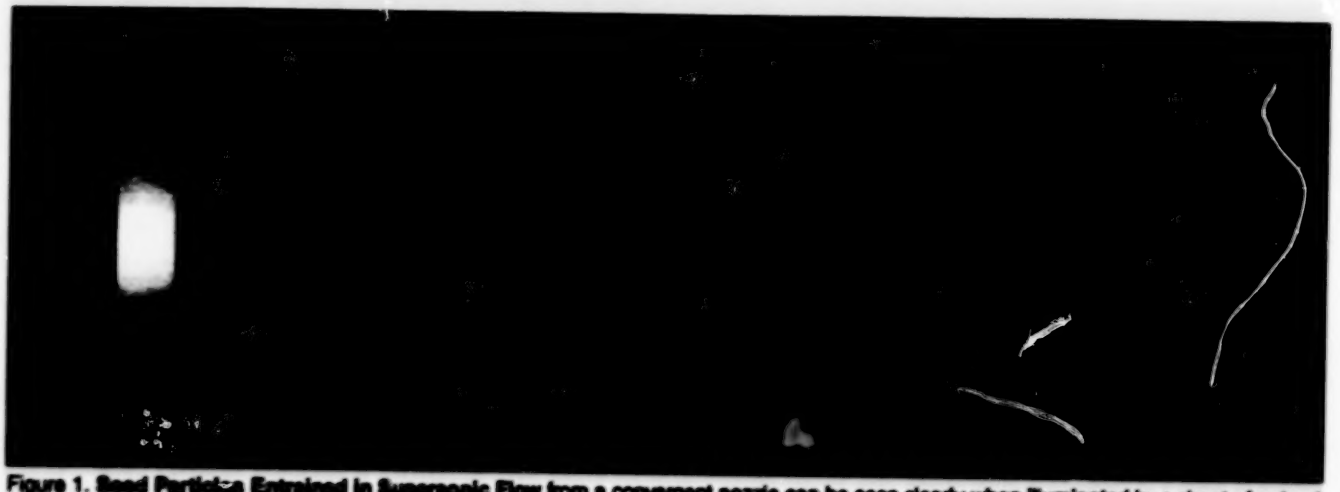

Figure 1. Seed Particles Entrained in Supersonic Flow from a convergent nozzle can be seen clearly when illuminated by a sheet of pulsed laser light. This is one of two images that are recorded a short time apart so that velocity vectors can be extracted from displacements between the first- and second-image positions of the particles.

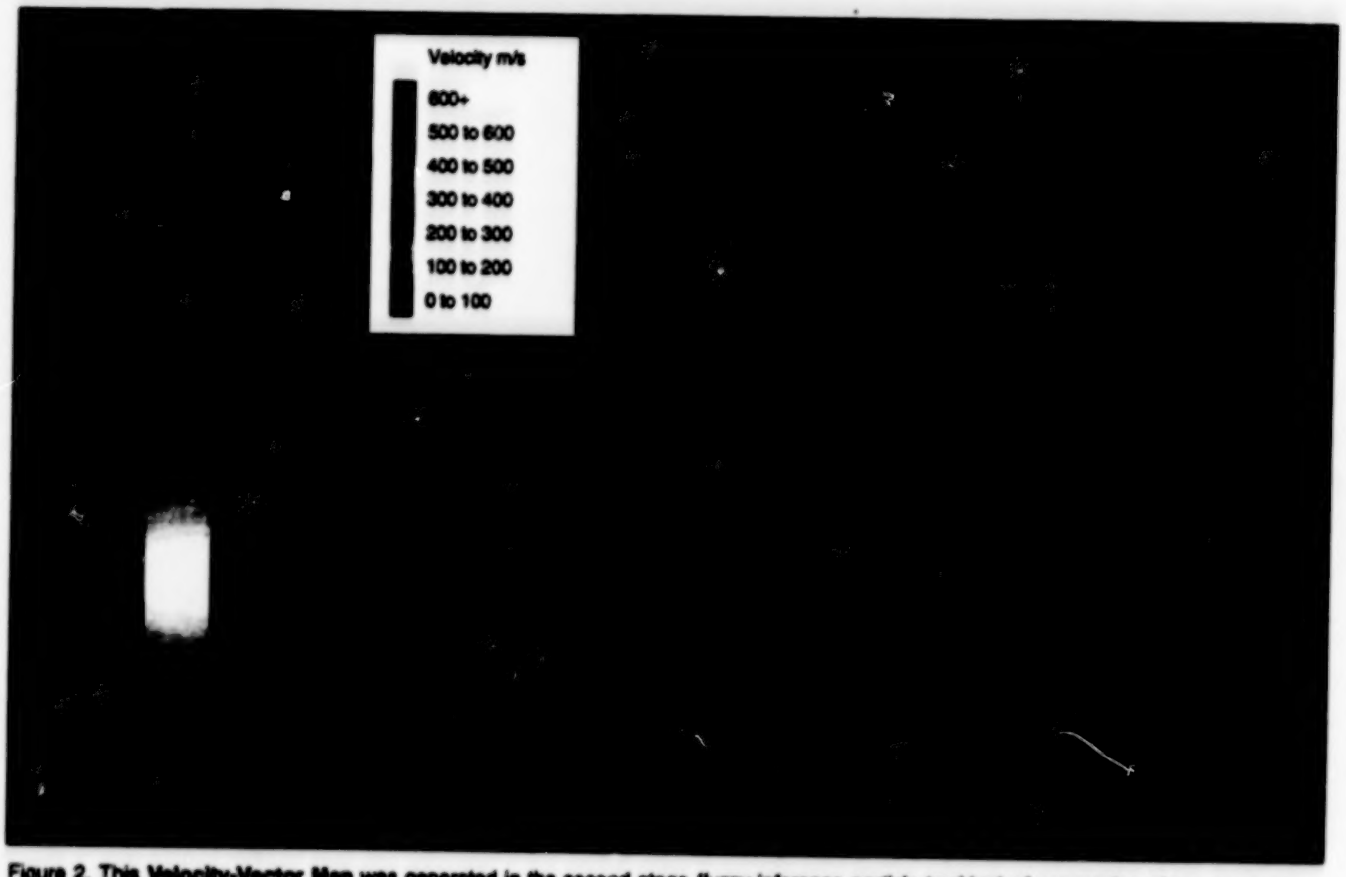

Figure 2. This Velocity-Vector Map was generated in the second stage (fuzzy-inference particle tracking) of processing of two consecutive images like that of Figure 1.

into equal-size regions, cross-correlations between corresponding regions are computed, and a fuzzy-logic inference engine is used to maximize the recovery of information from the correlation plane: Ideally, the peak of greatest amplitude on the correlation plane for each region would represent the average particle displacement and thus the average particle velocity in the region. However, when the seed density is low or there is out-of-plane particle motion, image noise, or a velocity gradient, a number of correlation peaks can arise. In an effort to select the correlation peak that represents the true velocity, a fuzzy inference operation is performed. The essence of this operation is to compare the velocity vectors of the five highest correlation peaks in each region with those of the five highest correlation peaks in each of the four surrounding regions and to select, for each region, the velocity vector most similar to the velocity vectors of the selected correlation peaks of the other regions according to a confidence-weighting numerical criterion. The justification for selecting velocity vectors on the basis of similarity to adjacent velocity vectors lies in the fundamental continuity of flow. Of course, because it represents velocities averaged over regions, the resulting velocity map inherently has low spatial resolution.

The second stage of the image-analysis process involves particle-tracking velocimetry, in which (1) the data from each frame are processed independently to

determine the particle-image centroids, (2) the centroid locations are used to determine candidate displacement vectors, and (3) velocity vectors are calculated by dividing the displacement vectors by the interexposure time. The major problem in selecting the displacement vectors is to determine which particle-image centroids in the second frame represent the subsequent positions of which particle-image centroids in the first frame. In the present method, this problem is solved by invoking two schemes, the first being a fuzzy-logic scheme with a selection criterion that is also based on continuity of flow; this scheme was described in "Particle-Tracking Velocimetry With Fuzzy Logic" (LEW-16205), *NASA Tech Briefs*, Vol. 20, No. 8 (August 1996), page 62.

In the second scheme, which also involves fuzzy logic, the low-resolution velocity map generated in the first stage is used as a further guide to selection of vectors: For each initial particle location, the four first-stage nearest-neighbor velocity vectors are used to compute a spatially weighted mean vector called the "benchmark" vector, which is then used in pairwise fuzzy comparison with all of the candidate vectors for the particle in question. The candidate vector most similar to the benchmark vector according to a confidence-weighting numerical criterion is selected as the velocity vector for that particle. This process is repeated for each initial particle location, yielding a high-resolution velocity-vector map (see Figure 2).

This work was done by Mark P. Wernet of **Lewis Research Center**. *Further information is contained in a TSP [see page 1].*

Inquiries concerning rights for the commercial use of this invention should be addressed to NASA Lewis Research Center, Commercial Technology Office, Attn: Tech Brief Patent Status, Mail Stop 7–3, 21000 Brookpark Road, Cleveland, Ohio 44135. Refer to LEW-16415.

BLANK PAGE

Fabrication Technology

Hardware, Techniques, and Processes

47 Forming Waveguide-Cooling Jackets by Extrusion

47 Arc-Burn-Suppression System for Manual Resistance Welding

BLANK PAGE

Forming Waveguide-Cooling Jackets by Extrusion

Fabrication time, cost, and difficulty would be reduced.

NASA's Jet Propulsion Laboratory, Pasadena, California

High-power waveguides with integral cooling jackets would be fabricated by extrusion, according to a proposal. At present, a waveguide with cooling jackets is fabricated by one of two alternative methods (see figure): (1) the waveguide and tubular cooling jackets are fabricated separately, then joined by soldering or brazing; or (2) the waveguide and its cooling jackets are formed in one piece by electrodeposition of metal on wax or aluminum mandrels with the cross sections of the waveguide and cooling jackets, then the mandrels are removed by melting or chemical etching. The first method is difficult, time-consuming, and expensive, and the discontinuities in thermal conductivity at the solder or braze joints in the cooling paths reduce cooling efficiency. In the second method, one obtains a single piece without thermal-conductivity discontinuities, but the second method is even more expensive and time-consuming, and is limited to materials that can be electrodeposited.

Fabrication of a waveguide and cooling jackets in one piece by extrusion would be easier, faster, and less expensive, in comparison with fabrication by the current methods. Like electrodeposition, extrusion would form the waveguide and cooling jackets as one piece, providing continuity of high thermal conductivity along the cooling paths and thus high cooling efficiency.

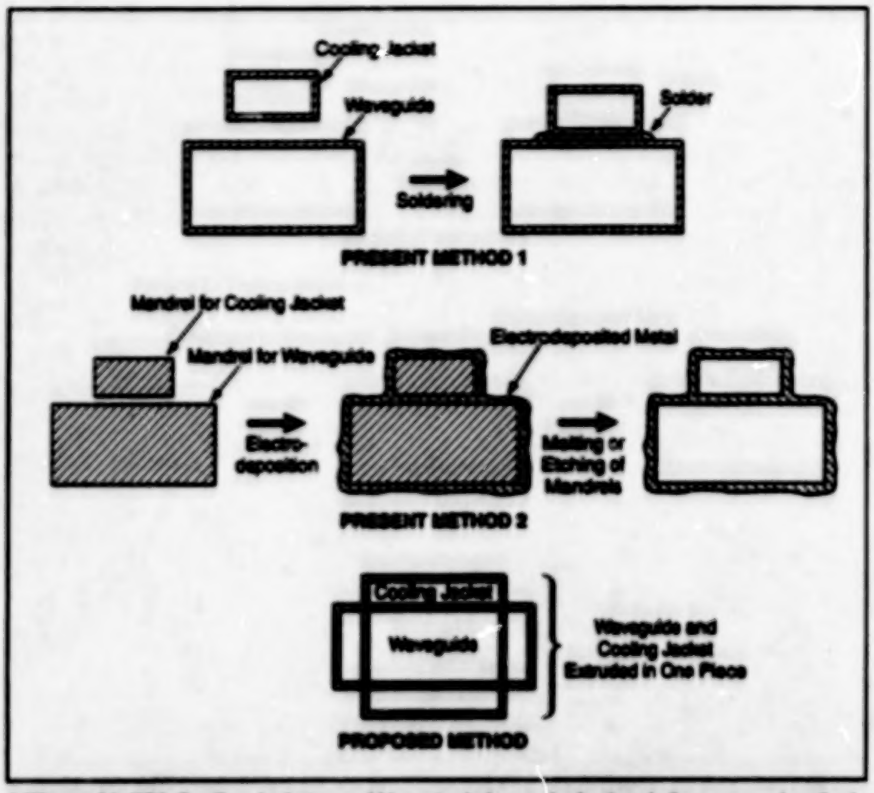

A Waveguide With Cooling Jackets would be extruded as a single piece in the proposed method.

This work was done by Raul M. Perez of Caltech for NASA's Jet Propulsion Laboratory. Further information is contained in a TSP [see page 1].

NPO-19680

Arc-Burn-Suppression System for Manual Resistance Welding

This monitor system prevents the formation of an arc column during weld operations.

Marshall Space Flight Center, Alabama

A weld-force monitor system is now being used to prevent arcing should there be a loss of contact between a weld electrode and the weldment during the resistance-welding process. Previously, resistance welding involved the manual application of the weld force. Slipping of the weldment during the welding operation often resulted in an arc, which damaged the weldment. Also, in previous welding processes, the achievement of proper welds depended on the skill and endurance of technicians.

The arc-burn-suppression system (see figure) incorporates a pressure transducer, which is mounted behind a low-mass collet assembly in a welding gun, to measure the welding force. A wide-band

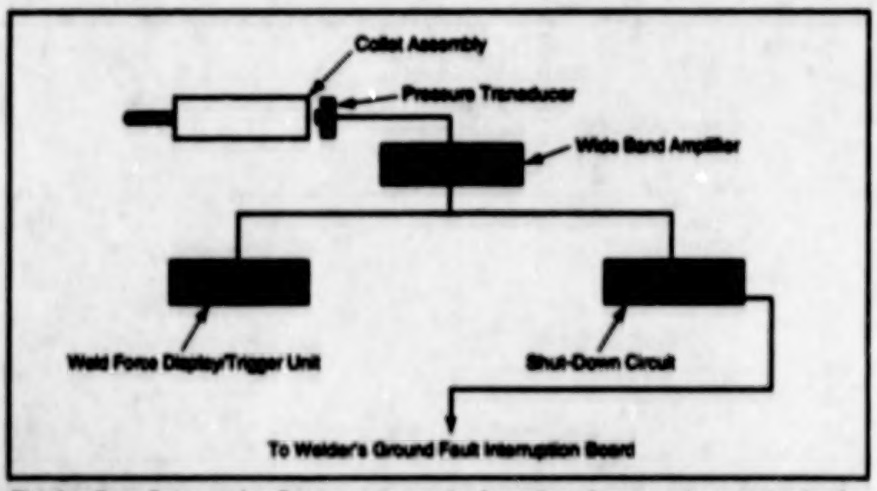

The Arc-Burn-Suppression System prevents the formation of an arc column at the tip of a weld electrode during the manual resistance-welding process.

amplifier drives a welding-trigger circuit and shuts down this circuit within a brief response time when it detects loss of contact.

The signal from the pressure transducer is sent to a wide-band amplifier. This amplifier provides a low-noise, high-gain input signal to a welding-force display unit, which triggers the welding sequence at the required welding force. The shutdown circuit, which is based on an LM311 integrated circuit, compares the incoming voltage from the wide-band amplifier with a reference or threshold voltage representative of the minimum allowable welding force. The shutdown circuit terminates the weld sequence when it detects that the force decreases to less than the minimum allowable welding force.

The originally specified response time of this arc-burn-suppression system was 12 milliseconds. However, the actual response time has proved to be less than 4 milliseconds. The trigger threshold of the shutdown circuit is adjustable to minimize the response time (normally set at 5 percent above the minimum weld force).

This work was done by Francis H. Nguyen, John Geddes, Gene Vanreenen, and Gregg Pilolles of Boeing North American, Inc., for **Marshall Space Flight Center.** *Further information is contained in a TSP [see page 1].*

Inquiries concerning rights for the commercial use of this invention should be addressed to the Patent Counsel, Marshall Space Flight Center [see page 1]. Refer to MFS-30127.

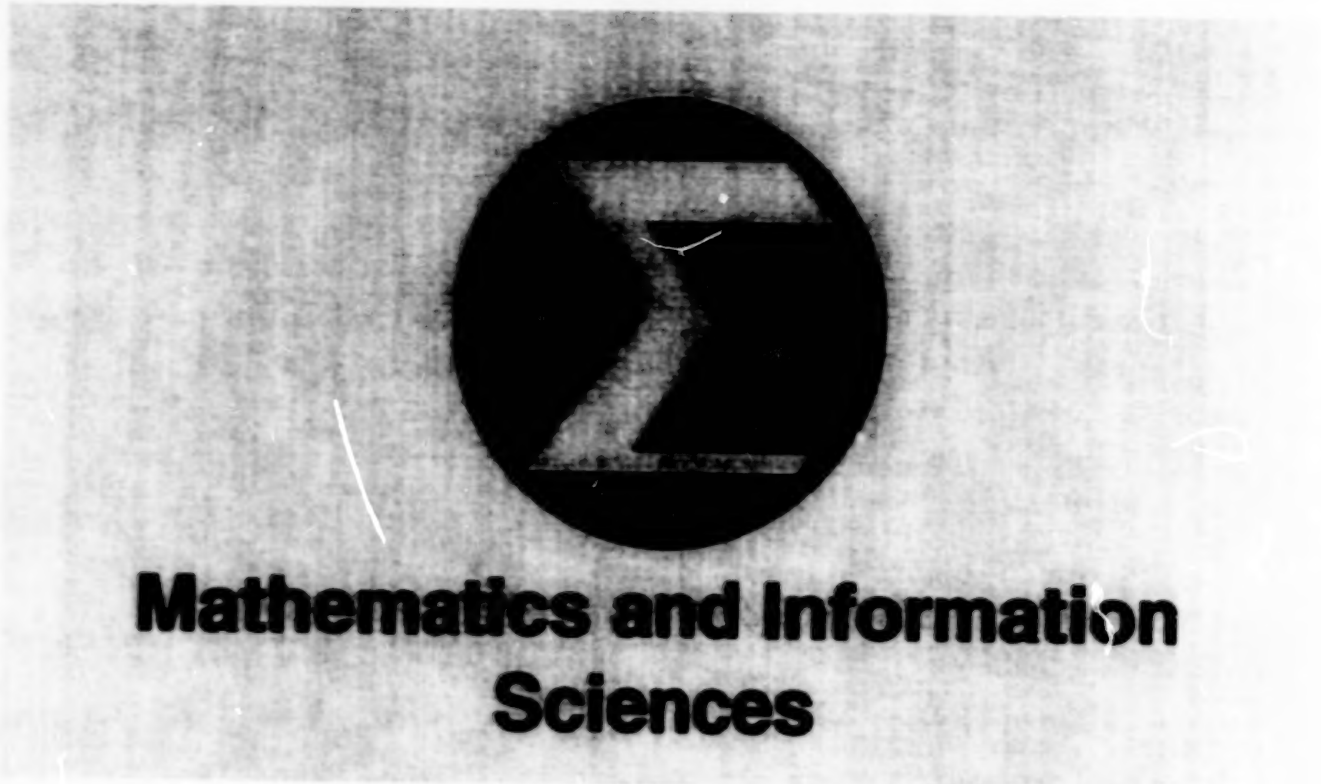

Mathematics and Information Sciences

Hardware, Techniques, and Processes

51 Computing Optimal Vibration-Sensor Configurations
52 Wavelet Analysis of Flight-Test Data on Aeroelasticity
54 Facilities Project Management System

BLANK PAGE

Computing Optimal Vibration-Sensor Configurations

Locations of sensors are chosen with the help of optimal full control synthesis.

Dryden Flight Research Center, Edwards, California

Choosing effective sets of sensor measurements is essential for designing controllers to satisfy stringent performance and robustness requirements. Often, control requirements are not anticipated at the design stages in the development of physical systems, and sensor configurations are chosen in an *ad hoc* manner. The choice of locations of vibration sensors for use in controlling or suppressing vibrations in flexible structures is an especially challenging problem because of the large number of vibration modes. Also, it is necessary to trade off (a) the number of sensors needed to observe a large number of closely spaced vibration modes against (b) the weight and cost of additional sensors.

The effectiveness of a sensor configuration can be analyzed by considering closed-loop-performance measures. Typically, in designing a controller, one uses feedback from each of a number of different configurations, seeking the configuration that maximizes these performance measures. A typical measure is the attenuation of vibration-mode responses. The optimal sensor configuration, according to this measure, is the one that maximizes the attenuation.

A method of computing optimal sensor configurations has been formulated by use of a method called "full control synthesis." Full control compensators are the optimal controllers for a given sensor configuration, since each state and error signal can be independently affected. The optimal full control synthesis is derived as a single linear matrix inequality condition, which can be solved by use of standard convex optimization algorithms.

Sensor configurations are chosen with this method by considering a set of feasible configurations. Globally optimal full control compensators are computed for each member of the set to determine the achievable performance level. The configuration associated with the highest performance for a full control compensator is optimal among the members of the set. There is no guarantee that this configuration will also be optimal for output feedback controllers; however, experiments indicate that this method can result in the choice of effective configurations for a physical system.

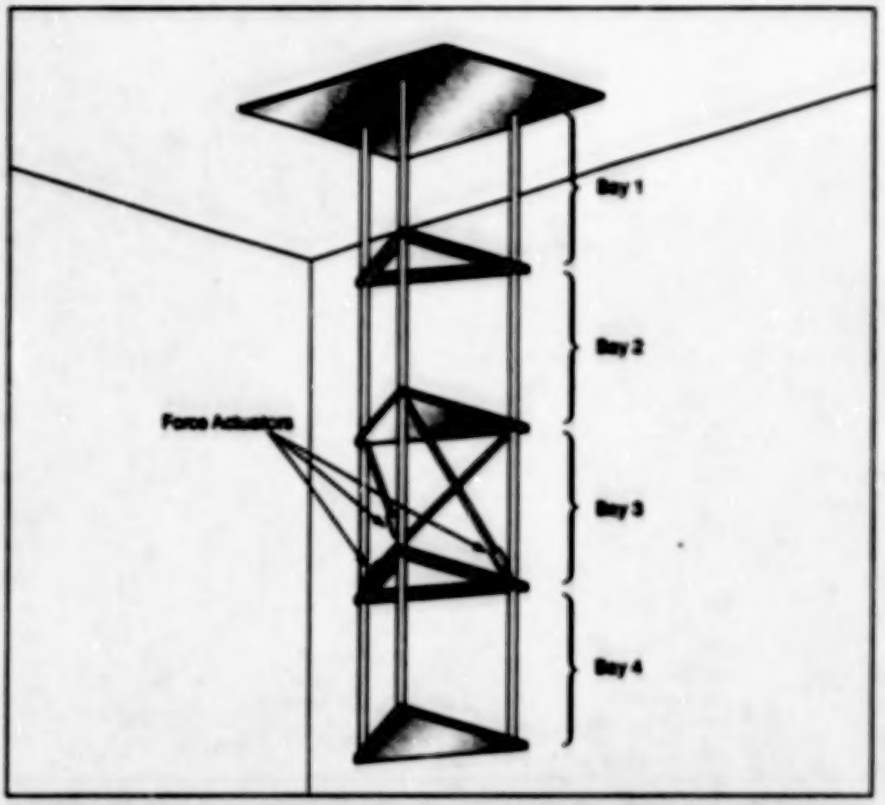

A Flexible Structure instrumented with force actuators and accelerometers was used to demonstrate the present method of selecting sensor locations to optimize active attenuation of vibrations.

The method has been used to determine accelerometer configurations for attenuating vibrations in a four-bay flexible aluminum structure at the University of Minnesota (see figure). Force actuators were located along diagonal beams in bay 3, while accelerometers were considered, to be located, alternatively, along the edges of plates in bay 3 or bay 4. The achievable predicted vibration-attenuation performance levels for each configuration with a full control compensator are shown in the table.

Output feedback controllers were implemented for each configuration. Experimental results demonstrated that configurations in which all accelerometers were in either bay 3 or bay 4 were nearly equally effective in attenuating vibrations, in agreement with the table. Also, bay-4 attenuation in the experiments was found to be better when feedback was obtained from bay-4 sensors (either alone or in combination with bay-3 sensors) than when feedback was obtained from bay-3 sensors only; this observation correlates with the predictions in the table.

Feedback Accelerometers	Bay-3 Performance	Bay-4 Performance
$3_1, 3_2$	1.379	3.031
$3_1, 3_2, 3_3$	0.269	0.719
$4_1, 4_2$	1.641	3.656
$4_1, 4_2, 4_3$	0.269	0.511
$3_1, 4_1$	3.281	1.312
$3_1, 4_2$	1.641	0.609

Performance Levels, in terms of vibrational-response levels (in g units of acceleration) as they would be measured in bays 3 and 4, were predicted for various accelerometer configurations. Each numerical symbol X_i denotes a sensor on the ith plate edge in bay X.

This work was done by Rick Lind of **Dryden Flight Research Center** *and Gary Balas and Volkan Nalbantoglu of the University of Minnesota. Further information is contained in a TSP [see page 1].*

DRC-97-35

Wavelet Analysis of Flight-Test Data on Aeroelasticity

Wavelet analysis offers advantages over Fourier analysis.

Dryden Flight Research Center, Edwards, California

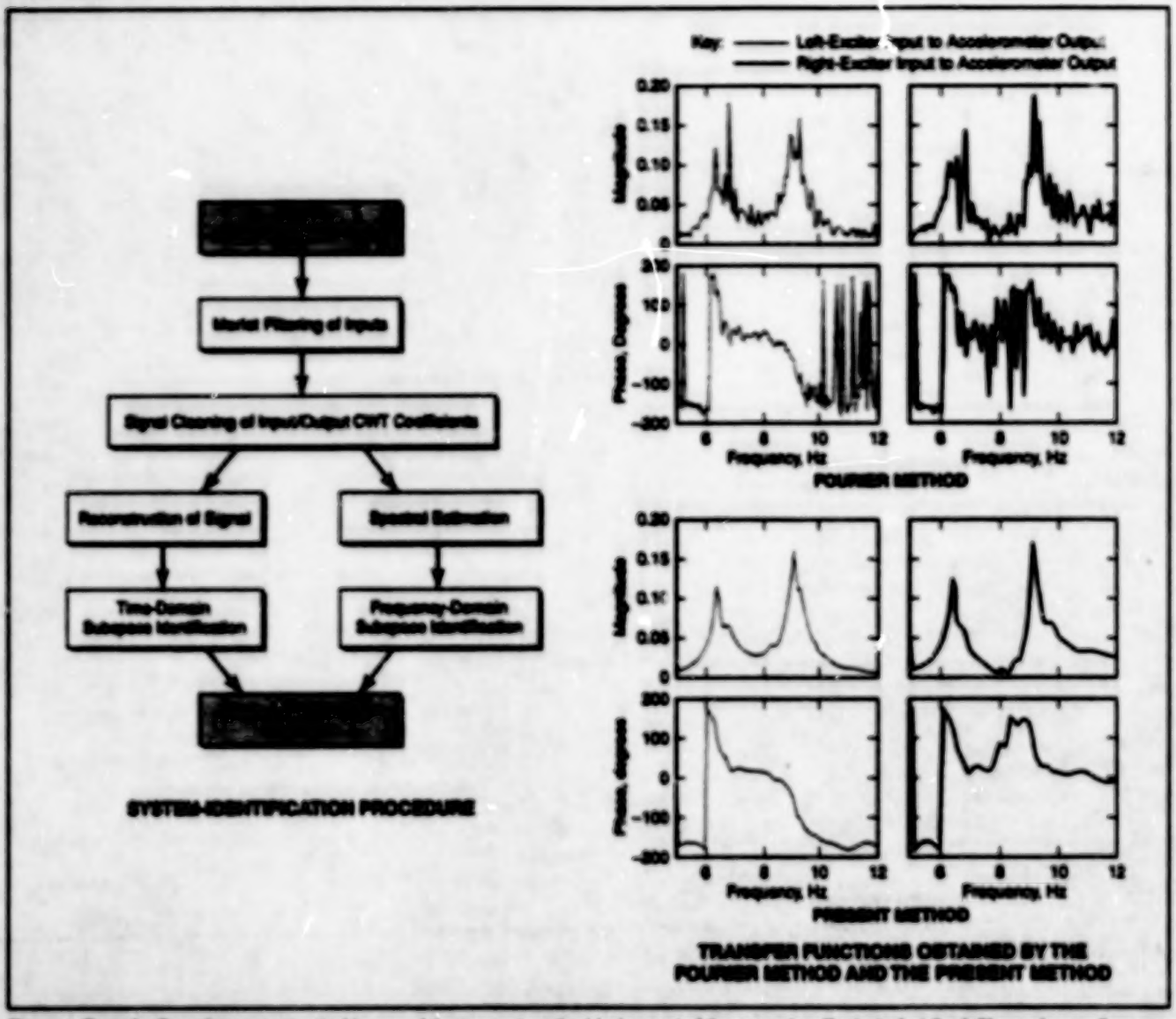

Figure 1. Transfer Functions constructed by use of the present method (using part of the procedure illustrated at the left) are cleaner than are those obtained by Fourier techniques.

A method of computational filtering enables the removal of distortions from flight-test data. The method is built upon and adapts the methods of wavelet-transform analysis to the particular test data. Although this method does not depend on the type of test data or other data to be analyzed, the initial application was to aeroelastic-flight-test data (e.g., accelerometer readings) generated with the help of structural-vibration-excitation systems on the F/A-18 Systems Research Aircraft (SRA) and the High Alpha Research Vehicle (HARV). Such excitation systems are often essential for enabling system-identification algorithms to resolve stability trends from noisy measurements, inasmuch as atmospheric turbulence generally does not provide excitation of the type needed for determining vibration-mode characteristics.

In processing flight flutter data, one attempts to analyze the characteristics of the data in terms of times, shapes, amplitudes, frequencies, and durations of events in the data. Such analyses have traditionally been performed by use of classical Fourier techniques. However, Fourier techniques are suspect in the presence of the inherently transient nature of in-flight aeroelastic dynamics; this is because the basic Fourier-analysis assumptions of infinite duration and at least local periodicity make it impossible to represent adequately the intermittency, modulation (amplitude, phase, or frequency), nonperiodicity, non-stationarity, time-variance, and/or nonlinearity in the data.

Wavelets are versatile harmonic-analysis tools that combine both time and frequency representations into localized waveforms. Given a segment of experimental data, the wavelet transform is constructed by convolving a selected series of local waveforms with the data to identify correlated features or patterns in the signal represented by the data. The result is a set of wavelet coefficients that can be interpreted as multidimensional correlation coefficients. Features of shape, size, and location are naturally characterized by these waveforms and related coefficients.

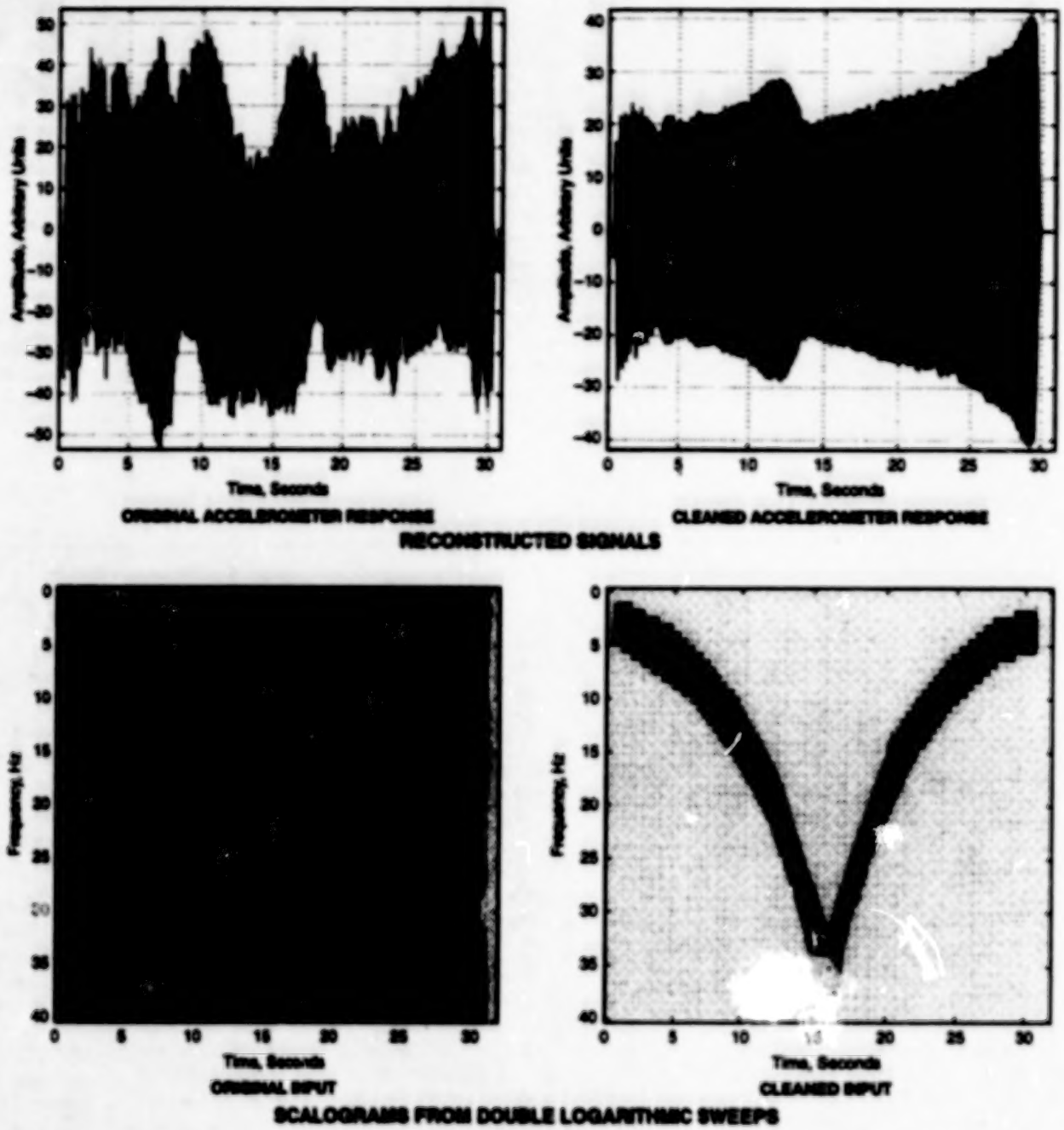

Figure 2. These Examples of Reconstructed Signals and Scalograms Illustrate the utility of the present method for cleaning signals.

The salient features of the original signal are reconstructed by exploiting the redundancy of the wavelets in the continuous wavelet transform (CWT). Unwanted time-frequency components are removed from the data by masking; that is, by setting the corresponding wavelet coefficients to zero. This procedure is followed to filter unwanted distortions and extract desired features from input (e.g., vibrational-excitation) and output (e.g., structural-vibrational-response) data. Extraction of features by this procedure offers advantages over traditional band-pass-filtering and thresholding techniques in that it results in the removal of unwanted features while leaving desired signal components intact.

Inasmuch as the F/A-18 structural excitations are essentially short-time sinusoids, a wavelet basis function could be expected to represent the characteristics of the excitation data. The Morlet wavelet was chosen as the basis function because of its clear interpretation in the frequency domain (Gaussian window) and time domain (locally periodic waveform) for the analysis of vibration data.

Transfer functions are used in structural dynamics to acquire state-space representations of the system modal dynamics, to determine stability estimates with standard methods, and to predict flutter boundaries with more advanced techniques. Traditional Fourier-transform methods involve averaging, windowing, and other procedures that often disguise important features in data. The present method includes a recipe to circumvent this deficiency by utilizing a wavelet-based feature-extraction filter to estimate cleaner transfer functions based on localization in frequency and time. The left part of Figure 1 schematically depicts a system-identification procedure (including a

procedure for constructing transfer functions) according to the present method.

The right part of Figure 1 presents an example of how the results achievable by use of the Morlet filter surpass those achievable by standard Fourier techniques. The Morlet processing affords an obvious improvement for identifying modal peaks in the presence of noise and in establishing well-defined phase response. Identification schemes used to extract modal data, state-space representations, and stability boundaries will perform better when the Morlet-filtering procedure is incorporated into them.

In reconstructing a signal, one uses the redundancy of the wavelets to estimate a time signal best approximated by the CWT. The real Morlet transform assures a reconstruction in phase with the original signal. The top part of Figure 2 presents an example of a reconstructed original signal and a reconstructed, cleaned version of the signal.

An example of filtering the undesired features of more-complicated input/output signal pairs in the time-frequency representation involves the use of a double logarithmic sweep from an excitation system. The bottom part of Figure 2 contains planer scalograms (maps of CWT coefficients) that pertain to this example. Harmonics from strain-gauge input measurements can be detected readily in the left scalogram. The presence of these harmonics indicates nonlinear excitervane response from rotating slotted cylinders at the ring tips. Such nonlinearity is deemed undesirable for subsequent analysis by linear state-space identification methods. Therefore, the input signal is processed by (a) extracting the desired time-frequency map from the left scalogram, yielding the right scalogram, then (b) reconstructing the time-domain input signal from the data represented by the right scalogram.

This work was done by Martin Brenner of **Dryden Flight Research Center** *and Eric Feron of Massachusetts Institute of Technology. Further information is contained in a TSP [see page 1].*
DRC-96-76

Facilities Project Management System

This software provides interactive access to accurate, timely information.

John F. Kennedy Space Center, Florida

The Facilities Project Management System (FPMS) computer program implements an automated data-base-management system for planning, budgeting, overseeing, and otherwise managing the construction of facilities under the NASA Facility Program. It provides a flexible data base, adaptable to all levels of project management at NASA installations and headquarters.

FPMS is a server-based, fully networked, interactive application program that utilizes the Microsoft FoxPro data-base-management software system as its core. FPMS is capable of interacting with commercial application programs (e.g., MS Word and MS Project), using object linking and embedding (OLE) technology to provide dynamic exchange of data between the data base and the commercial application programs. FPMS also incorporates the FoxPro report writer software, which provides viewing and printing capability for all standard reports and forms, as well as an ad hoc capability for end users to develop custom reports.

FPMS operates on a PC 486/33-compatible (or better) server at each NASA center and NASA Headquarters. It can be configured to work with either PC- or Macintosh-compatible workstations or both, and to use several types of networking software. FPMS also provides the functionality for electronic extraction and forwarding of information to accelerate status and financial reporting to headquarters. FPMS incorporates a flexible data-base structure to enable tracking at almost any level of detail desired by each NASA center, and makes possible a high degree of access control. The system can be designed to fit the flow of business information, making it possible to enter and/or update information as it becomes known and to view the information anytime before printing forms.

The primary functions offered on the FPMS main menu are denoted "planning," "management," "contracts," and "reports." Other menu selections denoted "file," "edit," "admin," "tables," and "help" provide maintenance capabilities in support of the primary functions. A navigational button screen has been implemented to assist users in maneuvering between modules. This button screen displays the primary functions needed by most users. Selecting any of the primary menu functions reveals a list of screens applicable to that function. By highlighting any entry in the list, the user can cause the screen thus selected to be displayed. Such functions as "edit," "save," "cancel," and "new" are activated by selecting the corresponding button at the bottom of the screen. A keyboard or mouse can be used to place the cursor on any input field to enter or modify data. Any of the standard reports can be selected from the "reports" menu and viewed on the screen or printed by selecting the print option. An ad hoc reporting capability in the "reports" menu enables users to develop their own reports and save report setups for repetitive use. FPMS utilizes an export capability where users can choose custom data configurations and export the data to spreadsheet, data-base, or text files. A "Data Warehouse" contortion of flat files provides a flatter, simpler view of the data for ad hoc reporting and data exporting.

During the development of FPMS, it was found necessary to develop new OLE software for integrating the commercial application programs. The word-processing and scheduling documents are stored in the general field of the FPMS data base. Key fields in the word-processing and scheduling documents are dynamically linked with data resident in the data base, so that updating a field automatically results in a corresponding update in any report or screen in which that field appears. FPMS software uses OLE functions to call the commercial application programs to work on the documents stored in the General Field in the data base. Such information as the scheduling date fields is also stored in the data base.

The "general field" data type is also used to support a graphics notepad feature. This feature allows the user to copy images, pictures, charts, and the like, into the FPMS data base for specific reporting functions as well as any ad hoc requirements. The users have the option of copying their own Gantt chart into the specific reporting fields or letting FPMS generate one automatically. The ad hoc graphics notepad field can be used in ad

hoc reports or export tasks, as determined by each of the centers. FPMS and the commercial applications are all accessed through selections from the FPMS main menu. Options on the FPMS menu include "start" modules that handle communication with outside application programs. Once the commercial application programs are loaded, the transition from FPMS to those programs is quick and efficient.

An Internet home page has been created to keep the NASA centers up to date with FPMS development. This home page contains a user-comments area, tips and tricks section, and a download-files section, where base tables, release notes, and other documentation are retrieved as files. New FPMS releases are also distributed using the FPMS home page.

This work was done by Patricia F. Hatch of **Kennedy Space Center** *and Dennis Weaver, Patricia N. Daniel, Lawrence A. Geiger Kenneth E. McMillan, Jr., Christina L. Walker, Brian W. Brumfield, Rosa Machado-Wilson, and Robin E. Zaches of I-NET. Further information is contained in a TSP [see page 1].*

Inquiries concerning rights for the commercial use of this invention should be addressed to the Patent Counsel, Kennedy Space Center [see page 1]. Refer to KSC-11779.

National Aeronautics and
Space Administration

END

12-22-99